

Delineation and Fine-Scale Structure of Active Fault Zones during the 2014-2023 unrest at the Campi Flegrei Caldera (Southern Italy) from High-Precision Earthquake Locations

Francesco Scotto di Uccio¹, Anthony Lomax², Jacopo Natale³, Titouan Muzellec⁴, Gaetano Festa¹, Sahar Nazeri⁵, Vincenzo Convertito⁶, Antonella Bobbio⁷, Claudio Strumia⁴, and Aldo Zollo⁴

¹Università di Napoli Federico II

²ALomax Scientific

³Dipartimento di Scienze della Terra e Geoambientali, Università degli Studi di Bari Aldo Moro

⁴University of Naples Federico II

⁵University of Naples Federico II, Naples (Italy)

⁶Istituto Nazionale di Geofisica e Vulcanologia, Osservatorio Vesuviano

⁷Istituto Nazionale di Geofisica e Vulcanologia

January 6, 2024

Abstract

In the past two decades, the central portion of Campi Flegrei caldera has experienced ground uplift of up to 15 mm/month, and a consequent increase in the rate, magnitudes and extent of seismicity, especially in the past two years. We use a new method for multi-scale precise earthquake location to relocate the 2014-2023 seismicity and map in detail currently activated fault zones. We relate the geometry, extent, and depth of these zones with available structural reconstructions of the caldera. The current seismicity is mainly driven by the time-varying, ground-uplift induced stress concentration on pre-existing, weaker fault zones, not only related to the inner caldera, dome resurgence but also to ancient volcano-tectonic collapses and magma emplacement processes. The extent of imaged fault segments suggests they can accommodate ruptures up to magnitude 5.0, significantly increasing estimates of seismic hazard in the area.

1 **Delineation and Fine-Scale Structure of Active Fault Zones during**
2 **the 2014-2023 unrest at the Campi Flegrei Caldera (Southern Italy)**
3 **from High-Precision Earthquake Locations**

4
5 *Francesco Scotto di Uccio*¹, *Anthony Lomax*², *Jacopo Natale*³, *Titouan Muzellec*¹, *Gaetano*
6 *Festa*^{1,4}, *Sahar Nazeri*¹, *Vincenzo Convertito*⁵, *Antonella Bobbio*⁵, *Claudio Strumia*¹ and *Aldo*
7 *Zollo*¹

8
9 ¹ Department of Physics Ettore Pancini, Università di Napoli Federico II, Napoli, Italy

10 ² ALomax Scientific, Mouans-Sartoux, France

11 ³ Department of Earth and Geoenvironmental Sciences, Università di Bari “Aldo Moro”, Bari,
12 Italy

13 ⁴ Istituto Nazionale di Geofisica e Vulcanologia, Roma, Italy

14 ⁵ Osservatorio Vesuviano, Istituto Nazionale di Geofisica e Vulcanologia, Napoli, Italy

15 Corresponding author: Aldo Zollo (aldo.zollo@unina.it)

16
17 **Key Points:**

- 18 • High-precision location of 2014-2023 seismicity in Campi Flegrei images active fault
19 zones with unprecedented detail.
- 20 • From 2021 onwards the seismicity produces an elliptic pattern resembling that of the
21 1982-84 unrest phase of the caldera.
- 22 • Seismicity occurs along different volcano-tectonic structures including the inner ring
23 fault zone and faults bounding the Solfatara crater.

24 **Abstract**

25 In the past two decades, the central portion of Campi Flegrei caldera has experienced ground uplift
26 of up to 15 mm/month, and a consequent increase in the rate, magnitudes and extent of seismicity,
27 especially in the last two years. We use a new method for multi-scale precise earthquake location
28 to relocate the 2014-2023 seismicity and map in detail currently activated fault zones. We relate
29 the geometry, extent, and depth of these zones with available structural reconstructions of the
30 caldera. The current seismicity is mainly driven by the time-varying, ground-uplift induced stress
31 concentration on pre-existing, weaker fault zones, not only related to the inner caldera, dome
32 resurgence but also to ancient volcano-tectonic collapses and magma emplacement processes. The
33 extent of imaged fault segments suggests they can accommodate ruptures up to magnitude 5.0,
34 significantly increasing estimates of seismic hazard in the area.

35

36 **Plain Language Summary**

37 During the past two years, there has been a marked increase of ground uplift and number and size
38 of earthquakes at Campi Flegrei caldera. This increase in activity has raised concerns in the
39 population and public authorities about the impact of seismic activity on buildings and
40 infrastructure in the area and about the best actions to undertake during the seismic emergency to
41 reduce the risk. Additionally, the possibility of a future volcanic eruption is being considered,
42 although currently geochemical and geophysical monitoring shows no clear and unequivocal signs
43 of precursory phenomena. In this work we map the last decade of seismicity with high-precision
44 earthquake locations with the aim of unveiling the currently activated fault zones of the inner
45 caldera and assessing the potential hazard of earthquake ruptures along the delineated fault zone.
46 The results show an expanding, near-elliptical distribution of seismicity. The size of faults imaged
47 in the caldera suggest earthquakes up to magnitude 5.0 can occur, significantly increasing
48 estimates of seismic hazard in the area.

49

50 **1 Introduction**

51 The Campi Flegrei caldera, in Southern Italy is located nearby the one million people living in
52 wide metropolitan area of Napoli, making it the worldwide most densely urbanized volcanic area
53 (e.g., Charlton et al., 2020). During the past two decades, the central portion of Campi Flegrei
54 caldera experienced a sustained and continuous ground uplift, reaching rates of 15 mm/month,

74 main precursors to volcanic eruptions, and are one of the primary indicators of the initiation and
75 evolution of a magmatic intrusion episode (McNutt et al., 1996). Since errors in earthquake
76 locations may preclude clear understanding of the ongoing processes, the use of precise seismicity
77 relocation techniques is emerging as a valuable tool to provide a comprehensive view of activated
78 faults and fractures during volcanic unrest, such as at the Campi Flegrei caldera.

79 The Campi Flegrei volcano is characterized by a nested caldera structure (Figure 1a; Orsi et al.,
80 1996; Orsi, 2022), produced by two large explosive eruptions, referred to as the Campanian
81 Ignimbrite (CI) and the Neapolitan Yellow Tuff (NYT), at 39 ka and 14.5 ka, respectively (Silleni
82 et al., 2020; Orsi et al., 1992), whose boundaries are now mapped also offshore (Natale et al.,
83 2022b). Since the NYT, over 70 eruptions occurred within the caldera boundaries, clustered in
84 time (i.e., volcanic epochs; Di Vito et al., 1999) and space along the main structural features (e.g.,
85 Bevilacqua et al., 2015). Since 10.5 ka, the volcanic activity is remarkably coupled with a caldera
86 resurgence phenomenon broadly acting in the central sector (Natale et al., 2022a), and displaying
87 a bell-shaped deformation pattern regardless of the scale and the polarity (uplift/subsidence). This
88 is similar to what is observed during historical ground deformation episodes (Bevilacqua et al.,
89 2020; Vitale and Natale, 2023).

90 Volcanic unrest and eruptions in the caldera are accompanied by seismotectonic phenomena.
91 Precursory seismicity and ground deformation patterns preceding the last historical eruption of
92 Monte Nuovo in 1538 CE (Di Vito et al., 2016) are similar to those in the current activity of the
93 caldera (Del Gaudio et al., 2010; Osservatorio Vesuviano – INGV, 2023).

94 Due to the high volcanic and seismic risk, the Campi Flegrei volcano hosts a highly advanced,
95 permanent multiparametric monitoring system (Bianco et al., 2022), including a dense seismic
96 monitoring network (Figure 1a). A series of ground uplift-subsidence with seismic activity
97 (bradyseismic) episodes affected the central area of Pozzuoli since early 1950s (Del Gaudio et al.,
98 2010), with the two most rapid uplift phases occurred in 1970-72 and 1982-84, reaching a
99 maximum uplift of about 4 m at RITE station in 1984 (Figure 1b), and producing over 20000
100 shallow earthquakes overall (D’Auria et al., 2011), concentrated in the Solfatara-Pisciarelli area
101 (Isaia et al., 2021). A long subsidence phase occurred between 1985 and 2005, with a maximum
102 subsidence of 90 cm and relatively rare seismicity (Gaeta et al., 2003). Since 2005 a new, long-
103 term, monotonic uplift phenomenon started with unsteadily accelerating seismicity (Bevilacqua et
104 al., 2022), especially from 2014 onwards (Figure 1c), which has produced a clear increase in the

105 number of seismic events and of the maximum magnitude (Figure 1d). At the beginning of 2023
106 the uplift surpassed the maximum elevation achieved during the previous 1982-1984 crisis (Figure
107 1b). The cause of the bradyseismic episodes is still debated within the volcanological community
108 (e.g., Troise et al., 2019). The main hypotheses are that the deformation is either directly caused
109 by pressure and/or volume changes induced by magma emplacement and intrusion at shallow
110 depths beneath the caldera (Woo and Kilburn, 2010; Macedonio et al., 2014) or it is due to the
111 poroelastic response of the shallow hydrothermal system to changes in pore pressure and fluid
112 content (Bonasia et al., 1984; Bonafede, 1991; Todesco, 2021; Nespoli et al., 2023). The latter
113 could be driven by the periodic migration toward the surface of crustal fluids possibly generated
114 by degassing processes at the primary, sill-like magma reservoir detected at 8 km depth by seismic
115 reflection experiments (Zollo et al., 2008). In favor of this second hypothesis, a lack of detectable
116 amount of magma at shallow depths was reported by previous seismic reflection soundings,
117 associated with the absence of univocal geochemical and geophysical magma movement signs
118 from multi-parametric data acquired by the dense monitoring system of the caldera (Vanorio et al.,
119 2005; Battaglia et al., 2008).

120 Changes in the deformation rate during the last ten years correlate with the changes in seismicity
121 rate and maximum magnitude of recorded events. Specifically, since 2020 there has been an
122 acceleration of ground uplift in the Campi Flegrei caldera, reaching in September 2023 a rate of
123 1-1.5 cm/month (Figures 1c, 1d), accompanied by an exponential increase in the earthquake rate
124 to about 1000 events per month (Figure 1d). Most of the earthquakes in the caldera occur at depths
125 shallower than 3 km, with a near-elliptical distribution as from the reference catalogue of INGV
126 (National Institute for Geophysics and Volcanology; Figure 1a). Most events have duration
127 magnitude $M_d \leq 1$, though starting in early 2023 there is a general increase of the average
128 magnitude per month, including several events with $M_d \geq 3$ and a largest, $M_d 4.2$ earthquake,
129 occurred on September 27, 2023.

130 The occurrence of five $M_d 3.6+$ earthquakes during the period August 18 – October 2, widely felt
131 in the Campi Flegrei and Napoli metropolitan area, raised a great concern in the population and
132 civil protection authorities about the earthquake risk related to the volcanic activity. Given the
133 high-density urbanization of the area, it is therefore important to understand the impact, including
134 potential damage, to buildings and infrastructures caused by the repeated occurrence of small to
135 moderate, shallow-depth events generated by the accelerating ground uplift.

136 In this study, we obtained multi-scale, high-precision relocations of the ongoing seismicity,
137 allowing to identify, with unprecedented detail, the location and geometry of the activated
138 structures during this crisis in the central area of the caldera. We used these new results along with
139 mapped surface faults and fractures and other geophysical information to better understand the
140 mechanics of earthquake faulting in relation to the caldera resurgence and other volcanic
141 phenomena, with the aim of identifying zones where future, larger magnitude earthquake can
142 potentially occur.

143

144 **2 Event Dataset**

145 We used P and S arrival-times from the earthquake catalogue provided by the INGV – Osservatorio
146 Vesuviano from 01/01/2014 to 14/11/2023 (Figure 1a), available at
147 <https://terremoti.ov.ingv.it/gossip/flegrei>. Phase arrivals and associated relative uncertainties and
148 event duration magnitudes M_d from only the fully located events in the catalogue (8292
149 earthquakes) are used. For the selected events, M_d ranges between -1.1 and 4.2, with the M_d 4.2
150 event (2023-09-27 01:35:34) having the largest number of phase arrival times (18 P and 6 S picks).
151 Events with lower magnitude ($M_d < 2$) typically show 6 to 10 P, 2 to 4 S arrival times. We also
152 extracted arrival times from 18 stations of the INGV national network (yellow and red triangles in
153 Figure 1a), located within 15 km from the catalogue epicentres. For the same set of events, we also
154 recovered vertical component waveforms from 9 velocimetric stations available on EIDA portal
155 (<https://eida.ingv.it>; red triangles in Figure 1a). We extracted waveforms in the time window from
156 10 s before to 45 s after the event origin time and decimated the traces to a sampling frequency of
157 50 Hz.

158

159 **3. High-precision earthquake location**

160 We obtained multi-scale, high-precision earthquake locations with a new procedure based on the
161 NonLinLoc location algorithm (Lomax et al., 2000; Lomax et al., 2014; NLL hereafter) which
162 produces an a-posterior probability density function (PDF) in 3D space for hypocentre location.
163 The new procedure, NLL-SSST-coherence (NLL-SC), combines source-specific, station travel-
164 time corrections (SSST) with stacking of PDFs, probabilistic location for nearby events based on
165 waveform similarity (Lomax and Savvaidis, 2022; Lomax and Henry, 2023).

166 In a first relocation step, NLL-SC iteratively develops SSST corrections on collapsing length scales

167 (Richards-Dinger and Shearer, 2000; Lomax and Savvaidis, 2022), which can greatly improve,
168 multi-scale relative location accuracy and clustering of events. In a second relocation step, NLL-
169 SC reduces finer scale relative errors by consolidating information across locations based on
170 waveform coherency between the events (Lomax and Savvaidis, 2022). This procedure is based
171 on the concept that if the waveforms for two events at a station are very similar (e.g., have high
172 coherency) up to a given frequency, then the distance between the two events is small relative to
173 the wavelength corresponding to that frequency (e.g., Geller and Mueller, 1980; Poupinet et al.,
174 1984). In this study we apply NLL-SC up to a frequency of 10 Hz, giving improved relative
175 location accuracy down to ~ 100 m scale. See the Supporting Information (Text S1) for more details
176 on the location procedure, velocity model (Figure S2) and processing parameters used in this study.

177

178 **4. Results**

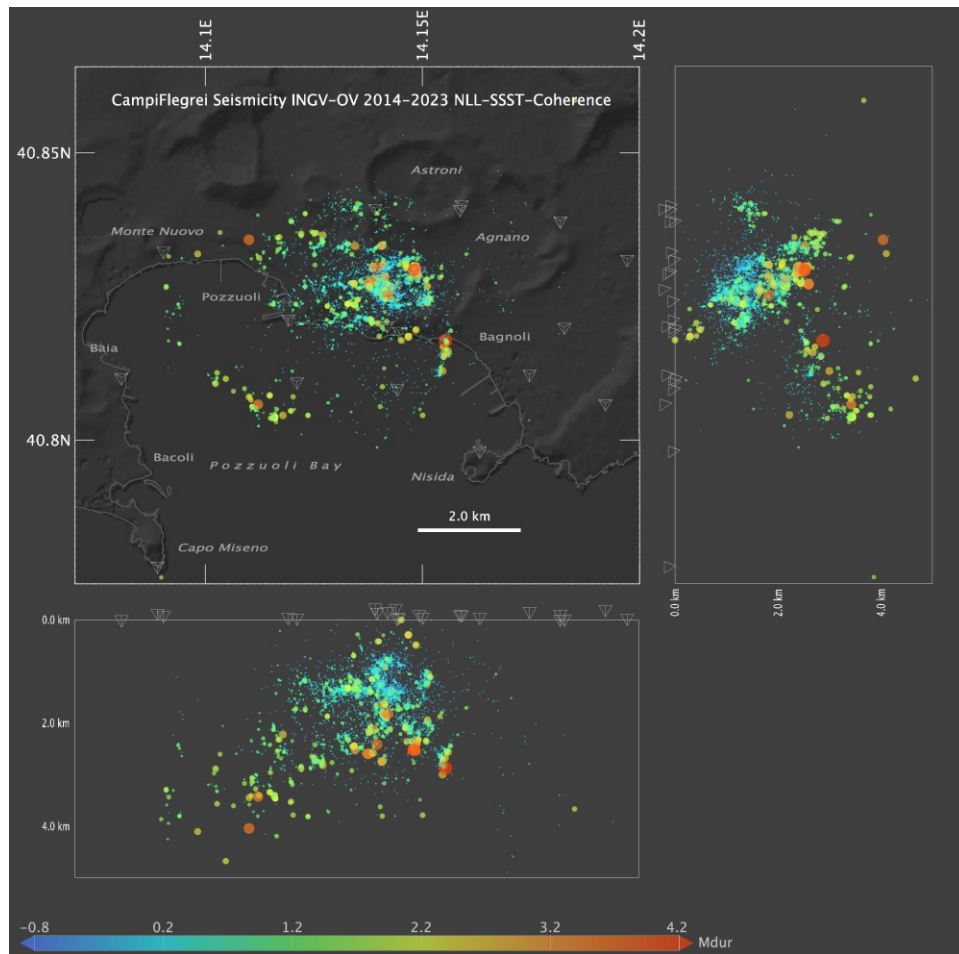
179 The high-precision NLL-SC locations delineate several clusters and alignments of seismicity
180 produced during the ongoing unrest at Campi Flegrei. Most of the seismicity concentrates in the
181 shallow region around the Solfatara-Pisciarelli area (cyan-green dots in Figure 2). Here, epicenters
182 define an $\sim 1 \times 1$ km, horseshoe-shaped structure, opened and deepening toward the northeast
183 beneath the Agnano Plain, and slightly larger than the ~ 0.5 km diameter of the Solfatara crater.
184 Smaller-scale seismicity clusters, with a typical size of 100-300m, occur south and southwest of
185 Solfatara, along the coast toward the center of Pozzuoli and the location of RITE station. This area
186 has been active since 2014 (Figure 3), although the seismicity has intensified during the last three
187 years.

188 The most recent magnitude Md 3.6+ events, except for the largest magnitude Md 4.2 earthquake,
189 also occurred in the Solfatara-Pisciarelli area, beneath the horseshoe-shaped seismicity, at depths
190 between 2 and 3.5 km. Northwest of the Solfatara crater, seismicity depicts a E-W trending, 1.5-
191 2.0 km long structure composed of event cluster at depths comparable to that of the major events
192 in the Solfatara.

193 Southeastward, off the coast of Bagnoli, a ~ 1 km long, sub-vertical alignment trending just E of N
194 is well defined by the relocated seismicity. This alignment contains the largest recorded event (Md
195 4.2), which ruptured an area of 800-1200 m², according to the calculated source radius (Figure S1
196 of Supporting Information). Further offshore to the southwest the seismicity occurs at greater
197 depths, down to ~ 4 km, and forming a WNW oriented alignment offshore of Bacoli, and a N-S

198 alignment off the coast of Monte Nuovo. Overall, this seismicity forms an elliptical shape,
 199 punctuated by the lineations and clusters containing the larger magnitude ($M_d > 3$) events.

200



201

202 **Figure 2:** Relocated NLL-SC seismicity 2014-2023. Circles – color coded according to the magnitude
 203 duration - show earthquakes with duration magnitude $M_d \geq -1.0$ and ellipsoid major axis ≤ 2.0 km (7212
 204 of 8274 total relocated events); symbol size is proportional to magnitude. Tetrahedrons show subsets of
 205 stations from Figure 1a used for relocation.

206

207 The evolution of the seismicity over time (Figures 1d and 3) shows an increasing of the number of
 208 events and maximum magnitude. Moreover, while in the period 2014-2019 seismicity occurred at
 209 shallow depths (most of these events have depth < 2 km) and concentrated in the Solfatara-
 210 Pisciarelli area, during 2019-2023 the seismicity deepens, extends offshore and increases in
 211 maximum magnitude. During the last two years (2022-2023), the seismicity spreads to a larger
 212 area, forming the elliptical, ring-like structure, extending from inland north of Solfatara

213 southwards through Bagnoli, eastwards towards Bacoli and northward towards Monte Nuovo.

214

215 **5. Discussion**

216 The precisely located NLL-SC seismicity delineates the fault zones activated during the ongoing
217 seismic crisis at Campi Flegrei (Figure 2) with greater detail as compared to the raw bulletin dataset
218 (Figure 1a). Accurate delineation of the structures enables an improved interpretation of the fault
219 activation mechanisms in relation with the spatial stress variability and concentration as caused by
220 the extended ground uplift phenomenon. The multi-scale station corrections and waveform-
221 coherence based hypocenter consolidation of NLL-SC achieves a location precision of 100 m or
222 less, which is necessary to image faulting structures in a complex, multi-kilometer scale volcanic
223 environment such as Campi Flegrei.

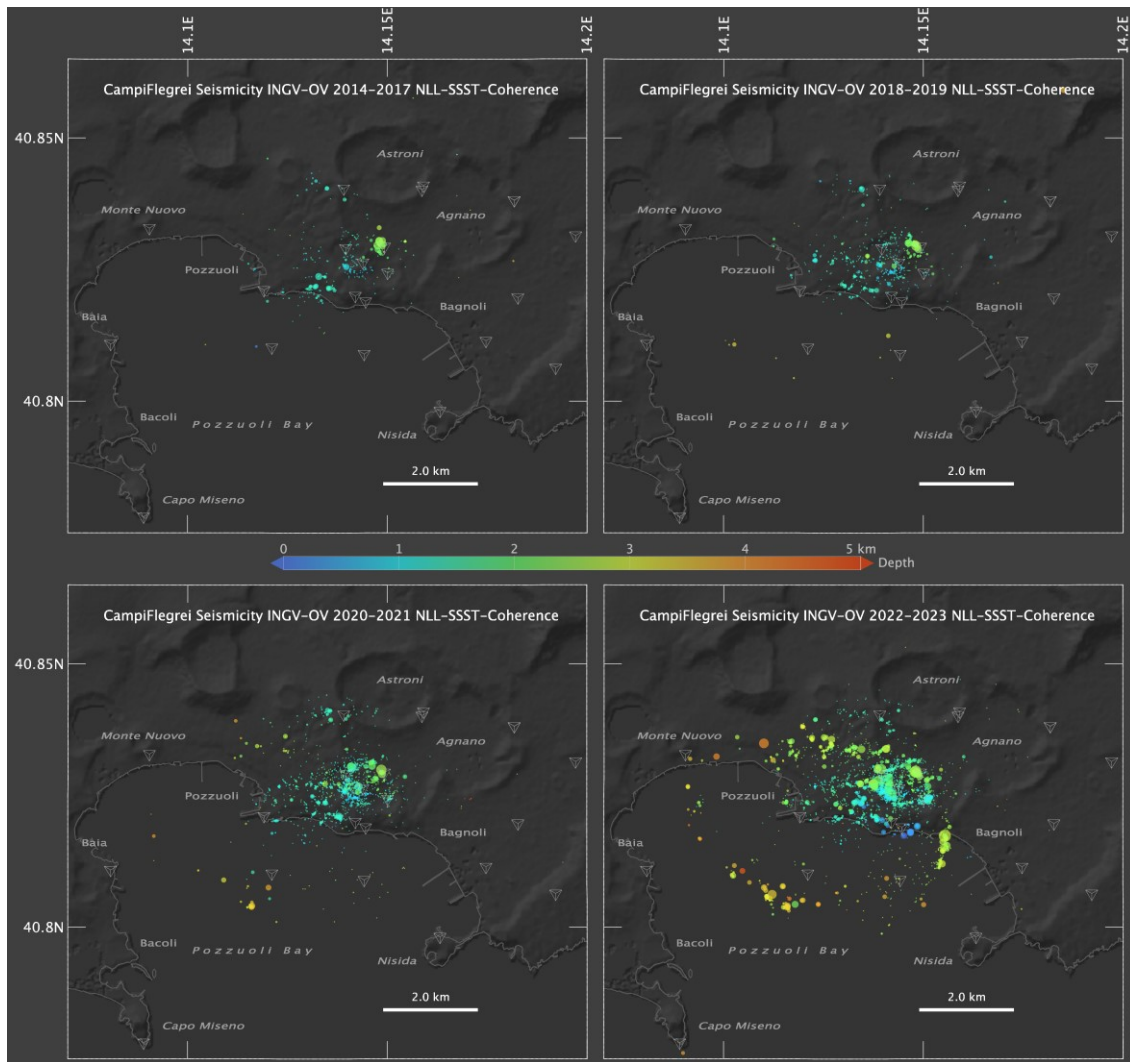
224 The spatiotemporal activation of shallow crustal volumes during 2014-2023 within the inner
225 caldera is shown by the relocated seismicity (Figure 3 and Supporting Information Video S1).

226 In the period 2014-2019 a low seismicity rate is observed (Figure 1c), mostly characterized by
227 small magnitude ($M_d < 2$) events occurring at depths shallower than about 3 km (Figure 3). These
228 events are located within a 1-2 km radius from the Solfatara crater which hosts, together with the
229 adjacent Pisciarelli fumarolic field, the most vigorous hydrothermal activity in the caldera
230 (Chiodini et al., 2017; Tamburello et al., 2019).

231 Overall, the variations in rate and magnitude of seismicity over time occur simultaneously with
232 changes in ground uplift rate of growth as observed at the station RITE in mid-2017, mid-2020
233 and end of 2022 (Figures 1c, d). Uplift velocity rather than cumulative uplift seems to control
234 localized seismicity production with the progressive activation of relatively long fracture zones at
235 the margin of the uplifting resurgent dome (Bevilacqua et al., 2022; Tramelli et al., 2022).

236 The spatial distribution of relocated seismicity (Figure 4) allows for an integrated geo-structural
237 interpretation based on recent evidence and reconstructions. The near-elliptical shape formed by
238 the seismicity since 2021 (Figure 4) resembles that of the 1982-84 crisis, whose seismicity
239 distribution has been related to a central collapsed portion of the caldera in studies (Barberi et al.,
240 1991; De Natale et al., 2006), which also considered results of gravity and magnetic surveys (Rosi
241 and Sbrana, 1987).

242



243
 244 **Figure 3:** Spatiotemporal evolution of the seismicity in periods 2014-2017, 2018-2019, 2020-2021 and
 245 2022-2023. Circles show earthquakes with magnitude $M_d \geq -1.0$ and ellipsoid major axis ≤ 2.0 km; symbol
 246 size is proportional to magnitude. Tetrahedrons show stations used for relocation.

247
 248 However, this hypothesis is contradicted by the geological evidence of a nested caldera structure
 249 (e.g., Orsi et al., 1996; Di Vito et al., 1999). Only a part of the relocated seismicity, occurring in
 250 the offshore sector (Feature A in Figure 4), is compatible with the caldera ring fault zone (e.g.,
 251 Sacchi et al., 2014; Steinmann et al., 2018). In a recent interpretation of high-resolution, seismic
 252 reflection profiles offshore of the caldera, Natale et al. (2022b) present evidence for a composite,
 253 ring-fault zone. This fault zone has an inner-ring confining from the west to the south-east the
 254 resurgent dome area, this latter being affected by a dense array of high-angle NE-SW to NNE-
 255 SSW trending, km-size collapse faults that cut the shallow marine sediments (Natale et al., 2020).

256 Several authors differentiate the inner-ring structure from the medial and outer ring fault systems,
257 whose expression at depth matches well the annular high-P-velocity, high-density body, imaged
258 by the 2001 active seismic tomography experiment and identified as the buried rim of the caldera
259 (Zollo et al., 2003; Judenherc and Zollo, 2004; Battaglia et al., 2008; Dello Iacono et al., 2009).

260 Only the deepest offshore seismicity, between 3-5 km depth, appears to fit and approximate the
261 downward propagation of the south-western inner ring fault (Figure 4a, f), where the most frequent
262 dip angles are between 60-80° (Natale et al., 2022b). This is consistent with a steep (~70°) inward-
263 dipping fault structure that justifies the 1.2 km spatial gap between the surface projection of the
264 mapped inner-ring fault and the 4 km deep epicenter locations. The focal mechanism solution (see
265 Supporting Information, Text S3) is consistent in terms of strike and dip of the nodal plane,
266 although with right-lateral kinematics (event 6 in Figure 4).

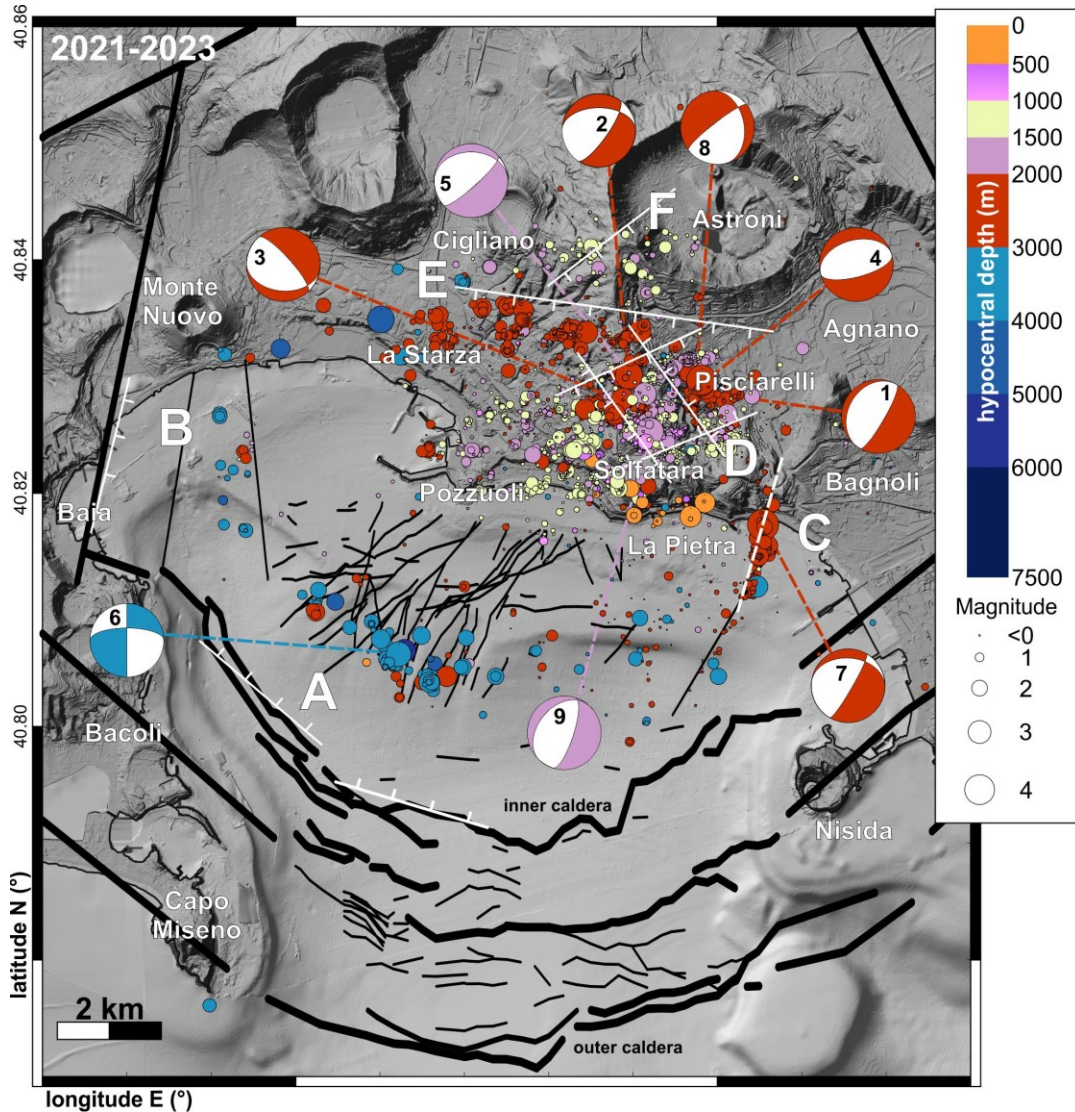
267 Activation of the Baia section (Feature B in Figure 4) of the inner ring fault (Vitale and Natale,
268 2023) can explain the seismicity off the coast of Monte Nuovo (between 3-5 km depth), where
269 underwater high-temperature hydrothermal manifestations occur (Di Napoli et al., 2016). The
270 more scattered and shallower seismicity could be related to high-angle faults as detailed in Natale
271 et al. (2022b), also involved by hot fluid uprise (Carlino et al., 2016).

272 Of particular interest is the near N-S trending sub-vertical fault structure just offshore La Pietra
273 (Feature C in Figure 4), generating the largest magnitude (Md 4.2) recorded event up to now during
274 the crisis, and overall producing earthquakes between 2-4 km depth. This structure has not been
275 identified previously as it lies in a region where no deep-penetrating seismic reflection profiles are
276 available. From spectral modelling of seismic displacement records the average seismic moment
277 and corner frequency of the event indicate a southward rupture extending over ~800-1200 m²
278 (Figure and Text S1 in Supporting Information), which is consistent with the area filled by nearby
279 seismicity (Figure 4), and the calculated focal mechanism (event 7 in Figure 4). However, given
280 the near-vertical dip angle and related hypocenter uncertainty, this fault structure could be dipping
281 to the east or to the west.

282 The offshore La Pietra fault structure illuminated by the relocated seismicity, represents a new
283 seismogenic feature in the caldera as compared to the 1982-84 crisis (e.g., Orsi et al., 1999). This
284 feature falls in the eastern portion of the near-elliptical seismicity pattern (Figure 4). The stress
285 drop estimated for the Md 4.2 event (2-3 MPa) in this structure is large in relation to the depth of

286 the structure, suggesting a high strength of rocks in the shallow caprock or underlying basement
 287 (Vanorio and Kanitpanyacharoen, 2015).

288



289 **Figure 4.** Simplified structural map showing the relationship between the epicentral distribution of
 290 relocated seismicity in the 2021-2023 period with the elliptical pattern and the main volcano-tectonic
 291 structures known in literature. Focal mechanisms solutions for selected 2023 Md>3 events are shown
 292 (details in Figure S3), with their color coded by depth.

294

295 Despite the moderate size of the event, the high stress drop acting over a small size asperity may
 296 be responsible for large peaks in the observed ground motion amplitudes (maximum recorded PGA
 297 of 0.3 g; see <http://shakemap.ingv.it/shake4/> archive.html).

298 In the Solfatara area (Figure 4, Feature D) the relocated seismicity matches well several fault arrays
299 mapped in the surface and subsurface geology. These fault arrays are related to the maar-diatreme
300 structure of Solfatara crater, whose polygonal shape is due to the presence of main NW-SE and
301 NE-SW faults, locally cross-cut by smaller E-W faults (Diamanti et al., 2022), and also exposed
302 at Pisciarelli fumarole field within the western rim of Agnano caldera (Isaia et al., 2021). Hence,
303 the horseshoe distribution of seismicity deepening eastward (Isaia et al., 2021) fits well the
304 presence of such array faults at depth, which significantly affects the hydrothermal circulation in
305 the area (Troiano et al., 2019). The calculated focal mechanisms (Figure 4 and Supporting
306 Information Text S3) show nodal planes consistent with the mapped structures, as they are mainly
307 NE-SW trending (events 1, 2, 5 and 8), and subordinately E-W trending (event 4) and NW-SE
308 (event 3).

309 An approximately E-W trending fault bounds the distribution of the relocated seismicity NE of the
310 Solfatara crater (Figure 4, Feature E), on which a series of spatially and temporally correlated
311 seismicity bursts occurred between 2 and 3 km depths. This structure corresponds to a south-
312 dipping normal fault with a left-lateral component, with noticeable surface expression in Agnano
313 and Cigliano as recently depicted in Natale et al. (2023) and corroborated by structural field data
314 by Diamanti et al. (2022). The bursts of seismicity occur along a ca. 6 km-long structure, that to
315 the west reaches La Starza marine terrace (Vitale et al., 2019), representing the northern border of
316 elliptical seismicity.

317 The NE-SW seismicity alignment (Figure 4, Feature F) in the Astroni might be associated with
318 pressurized fluids moving along a NE-SW faults within the shallow (1-1.5 km) portion of the
319 hydrothermal system (Isaia et al., 2022), where increased hydrothermal activity has been detected,
320 as corroborated by microgravity data (Young et al., 2020).

321

322 **5. Conclusions**

323 The general elliptical distribution of the ongoing seismicity at Campi Flegrei caldera is mainly
324 driven by the stress concentration causative effect of a bell-shaped ground deformation pattern
325 with fracture zones that appear coherent with the ones activated during the 1982-84 unrest in shape
326 and location (Scarpa et al., 2022). However, new sectors have been activated during the present
327 unrest, at the eastern boundary, where the largest Md 4.2 event was caused by a km-size rupture
328 within the shallow (3 km) volcanic sedimentary layer. We found that several structures delineated

329 by the ongoing seismicity have correspondence in the geological shallow fault record, whose
330 formation was not related to the same volcanic-tectonic process (i.e., dome resurgence), but rather
331 generated by other, more energetic processes such volcano-tectonic collapses, magma intrusion
332 and migration.

333 In general, the stress changes caused by the ongoing uplift of the central caldera appear to
334 concentrate on weaker pre-existing structures that are reactivated by small-to-moderate, sub-
335 kilometeric fractures. All the Md 3.6+ earthquake ruptures, apart from the largest Md 4.2 event,
336 have nucleated along segments of the complex SW-NE and SE-NW fault system array at the
337 margins of the Solfatara crater. As for the Md 4.2 event, the evidence for relatively high stress-
338 drops and average slip (2-3 MPa, 3-5 cm see Supporting Information) suggests a possible effect of
339 fluid-driven, pore-pressure increase at these faults that could favor the development of larger size
340 fractures.

341 Considering the size of the structures mapped in this study and the stress drop estimated for the
342 main event (Text S1 of Supporting Information), these faults can accommodate earthquakes of
343 moment magnitude up to 5.0, both beneath the Solfatara and offshore, south of Pozzuoli,
344 significantly increasing the hazard in the area.

345

346 **References**

347 Barberi, F., Cassano, E., La Torre, P., & Sbrana, A. (1991). Structural evolution of Campi Flegrei
348 caldera in light of volcanological and geophysical data. *Journal of volcanology and*
349 *geothermal research*, 48(1-2), 33-49.

350 Battaglia, J., Zollo, A., Virieux, J., & Dello Iacono, D. (2008). Merging active and passive data
351 sets in travelttime tomography: The case study of Campi Flegrei caldera (Southern Italy).
352 *Geophysical Prospecting*, 56, 555–573. <https://doi.org/10.1111/j.1365-2478.2007.00687.x>

353 Bevilacqua, A., Isaia, R., Neri, A., Vitale, S., Aspinall, W. P., Bisson, M., Flandoli, F., Baxter,
354 P.J., Bertagnini, A., Esposti Ongaro, T., Iannuzzi, E., Pistolesi, M., & Rosi, M. (2015).
355 Quantifying volcanic hazard at Campi Flegrei caldera (Italy) with uncertainty assessment:
356 1. Vent opening maps. *Journal of Geophysical Research: Solid Earth*, 120(4), 2309-2329.

357 Bevilacqua, A., Neri, A., De Martino, P., Isaia, R., Novellino, A., Tramparulo, F. D. A., & Vitale,
358 S. (2020). Radial interpolation of GPS and leveling data of ground deformation in a
359 resurgent caldera: application to Campi Flegrei (Italy). *Journal of Geodesy*, 94, 1-27.

- 360 Bevilacqua, A., De Martino, P., Giudicepietro, F., Ricciolino, P., Patra, A., Pitman, E. B., Bursik,
361 M., Voight, B., Flandoli, F., Macedonio, G., & Neri, A. (2022). Data analysis of the
362 unsteadily accelerating GPS and seismic records at Campi Flegrei caldera from 2000 to
363 2020. *Scientific reports*, 12(1), 19175.
- 364 Bianco, F., Caliro, S., De Martino, P., Orazi, M., Ricco, C., Vilardo, G., Aquino, I., Augusti, V.,
365 Avino, R., Bagnato, E., Brandi, G., Caputo, A., Carandente, A., Chiodini, G., Cuoco, E.,
366 D'Alessandro, A., Dolce, M., Guardato, S., Minopoli, C., Sansivro, F., Santi, A., Scarpato,
367 G., Tramelli, A., & Castellano, M. (2022). The permanent monitoring system of the Campi
368 Flegrei caldera, Italy. In *Campi Flegrei: A Restless Caldera in a Densely Populated Area*
369 (pp. 219-237). Berlin, Heidelberg. Springer Berlin Heidelberg.
- 370 Bonasia, V., Pingue, F., & Scarpa, R. (1984). A fluid-filled fracture as possible mechanism of
371 ground deformation at Phlegraean Fields, Italy, *Bullettin of Volcanology*, 47(2), 313–320.
- 372 Bonafede, M. (1991). Hot fluid migration: An efficient source of ground deformation: Application
373 to the 1982–1985 crisis at Campi Flegrei-Italy, *Journal of Volcanology and Geothermal*
374 *Research*, 48, 187–198.
- 375 Carlino, S., Mirabile, M., Troise, C., Sacchi, M., Zeni, L., Minardo, A., Caccavale, M., Daranyi,
376 V., & De Natale, G. (2016). Distributed-temperature-sensing using optical methods: a first
377 application in the offshore area of Campi Flegrei caldera (Southern Italy) for volcano
378 monitoring. *Remote Sensing*, 8(8), 674.
- 379 Charlton, D., Kilburn, C., & Edwards, S. (2020). Volcanic unrest scenarios and impact assessment
380 at Campi Flegrei caldera, Southern Italy. *Journal of Applied Volcanology*, 9, 1-26.
- 381 Chiodini, G., Selva, J., Del Pezzo, E., Marsan, D., De Siena, L., D'Auria, L., Bianco, F., Caliro,
382 S., De Martino, P., Ricciolino, P., & Petrillo, Z. (2017). Clues on the origin of post-2000
383 earthquakes at Campi Flegrei caldera (Italy). *Scientific reports*, 7(1), 4472.
- 384 De Natale, G., Troise, C., Pingue, F., Mastrolorenzo, G., Pappalardo, L., Battaglia, M., & Boschi,
385 E. (2006). The Campi Flegrei caldera: unrest mechanisms and hazards. *Geological Society,*
386 *London, Special Publications*, 269(1), 25-45.
- 387 Del Gaudio, C., Aquino, I., Ricciardi, G.P., Ricco, C., & Scandone, R. (2010). Unrest episodes at
388 Campi Flegrei: a reconstruction of vertical ground movements during 1905-2009. *Journal*
389 *of Volcanology and Geothermal Research*, 195, 48–56.

- 390 Dello Iacono, D., Zollo, A., Vassallo, M., Vanorio, T., & Judenherc, S. (2009). Seismic images
391 and rock properties of the very shallow structure of Campi Flegrei caldera (southern Italy).
392 *Bulletin of Volcanology* 71, 275–284. <https://doi.org/10.1007/s00445-008-0222-1>.
- 393 Diamanti, R., Camanni, G., Natale, J., & Vitale, S. (2022). A gravitational origin for volcano-
394 tectonic faults in the Campi Flegrei caldera (southern Italy) inferred from detailed field
395 observations. *Journal of Structural Geology*, 161, 104671.
- 396 Di Napoli, R., Aiuppa, A., Sulli, A., Caliro, S., Chiodini, G., Acocella, V., Ciraolo, G., Di Vito,
397 M. A., Interbartolo, F., Nasello, C., & Valenza, M. (2016). Hydrothermal fluid venting in
398 the offshore sector of Campi Flegrei caldera: A geochemical, geophysical, and
399 volcanological study. *Geochemistry, Geophysics, Geosystems*, 17(10), 4153-4178.
- 400 Di Vito, M. A., Isaia, R., Orsi, G., Southon, J. D., De Vita, S., d'Antonio, M., Pappalardo, L., &
401 Piochi, M. (1999). Volcanism and deformation since 12,000 years at the Campi Flegrei
402 caldera (Italy). *Journal of Volcanology and Geothermal Research*, 91(2–4), 221–246.
403 [https://doi.org/10.1016/S0377-0273\(99\)00037-2](https://doi.org/10.1016/S0377-0273(99)00037-2)
- 404 Di Vito, M. A., Acocella, V., Aiello, G., Barra, D., Battaglia, M., Carandente, A., Del Gaudio, C.,
405 de Vita, S., Ricciardi, G. P., Ricco, C., Scandone, R., & Terrasi, F. (2016). Magma transfer
406 at Campi Flegrei caldera (Italy) before the 1538 AD eruption, *Scientific Reports*, 6(1), 1–
407 9.
- 408 Gaeta, F. S., Peluso, F., Arienzo, I., Castagnolo, D., De Natale, G., Milano, G., Albanese, C. &
409 Mita, D. G. (2003). A physical appraisal of a new aspect of bradyseism: The miniuplifts.
410 *Journal of Geophysical Research: Solid Earth*, 108(B8).
- 411 Geller, R. J., & Mueller, C. S. (1980). Four similar earthquakes in central California. *Geophysical*
412 *Research Letters*, 7(10), 821–824. <https://doi.org/10.1029/GL007i010p00821>
- 413 Isaia, R., Di Giuseppe, M. G., Natale, J., Tramparulo, F. D. A., Troiano, A., & Vitale, S. (2021).
414 Volcano-tectonic setting of the Pisciarelli fumarole field, Campi Flegrei caldera, southern
415 Italy: Insights into fluid circulation patterns and hazard scenarios. *Tectonics*, 40(5),
416 e2020TC006227.
- 417 Isaia, R., Di Giuseppe, M. G., Troiano, A., Avino, R., Caliro, S., Santi, A., & Vitale, S. (2022).
418 Structure and present state of the Astroni Volcano in the Campi Flegrei caldera in Italy
419 based on multidisciplinary investigations. *Geochemistry Geophysics Geosystems*, 23(12),
420 e2022GC010534.

- 421 Judenherc, S., & Zollo, A. (2004). The Bay of Naples (southern Italy): Constraints on the volcanic
422 structures inferred from a dense seismic survey. *Journal of Geophysical Research: Solid*
423 *Earth*, 109(B10).
- 424 Krischer, L., Megies, T., Barsch, R., Beyreuther, M., Lecocq, T., Caudron, C., & Wassermann, J.
425 (2015). ObsPy: A bridge for seismology into the scientific Python ecosystem.
426 *Computational Science & Discovery*, 8(1), 014003.
- 427 Lomax, A., Virieux, J., Volant, P., & Berge-Thierry, C. (2000). Probabilistic Earthquake Location
428 in 3D and Layered Models. In C. H. Thurber & N. Rabinowitz (Eds.), *Advances in Seismic*
429 *Event Location*, 18, 101–134. Springer Netherlands. [https://doi.org/10.1007/978-94-015-](https://doi.org/10.1007/978-94-015-9536-0_5)
430 [9536-0_5](https://doi.org/10.1007/978-94-015-9536-0_5)
- 431 Lomax, A., Michelini, A., & Curtis, A. (2014). Earthquake Location, Direct, Global-Search
432 Methods. In R. A. Meyers (Ed.), *Encyclopedia of Complexity and Systems Science* (pp. 1–
433 33). Springer New York. https://doi.org/10.1007/978-3-642-27737-5_150-2
- 434 Lomax, A., & Savvaidis, A. (2022). High-Precision Earthquake Location Using Source-Specific
435 Station Terms and Inter-Event Waveform Similarity. *Journal of Geophysical Research:*
436 *Solid Earth*, 127(1), e2021JB023190. <https://doi.org/10.1029/2021JB023190>
- 437 Lomax, A., & Henry, P. (2023). Major California faults are smooth across multiple scales at
438 seismogenic depth. *Seismica*, 2(1), Article 1. <https://doi.org/10.26443/seismica.v2i1.324>.
- 439 Lomax, A., & Scotto di Uccio, F. (2023). Relocated event catalog for 2014-2023 seismicity at
440 Campi Flegrei [Data set]. *Zenodo*. <https://doi.org/10.5281/zenodo.10259822>
- 441 Lomax, A. (2023). NLL-SC processing parameters for the relocation of the 2014-2023 Campi
442 Flegrei seismicity [Data set]. *Zenodo*. <https://doi.org/10.5281/zenodo.10260849>
- 443 Macedonio, G., Giudicepietro, F., D’Auria, L., & Martini, M. (2014). Sill intrusion as a source
444 mechanism of unrest at volcanic calderas. *Journal of Geophysical Research: Solid Earth*,
445 119, 3986–4000. <https://doi.org/10.1002/2013JB010868>
- 446 McNutt, S. R., Scarpa, R., & Tilling, R. I. (1996). Monitoring and mitigation of volcano hazards.
447 In *Berlin, Federal Republic of Germany, Springer-Verlag, Ch. Seismic monitoring and*
448 *eruption forecasting of volcanoes: a review of the state-of-the-art and case histories* (pp.
449 99-146)

- 450 Natale, J., Ferranti, L., Marino, C., & Sacchi, M. (2020). Resurgent dome faults in the offshore of
451 the Campi Flegrei caldera (Pozzuoli Bay, Campania): preliminary results from high-
452 resolution seismic reflection profiles. *Bollettino di Geofisica Teorica ed Applicata*, 61(3).
- 453 Natale, J., Ferranti, L., Isaia, R., Marino, C., Sacchi, M., Spiess, V., Steinmann, L., & Vitale, S.
454 (2022a). Integrated on-land-offshore stratigraphy of the Campi Flegrei caldera: new
455 insights into the volcano-tectonic evolution in the last 15 kyr. *Basin Research* 34 (2), 855–
456 882.
- 457 Natale, J., Camanni, G., Ferranti, L., Isaia, R., Sacchi, M., Spiess, V., Steinmann, L., & Vitale, S.
458 (2022b). Fault systems in the offshore sector of the Campi Flegrei caldera (southern Italy):
459 implications for nested caldera structure, resurgent dome, and volcano-tectonic evolution.
460 *Journal of Structural Geology*. 163:104723. <https://doi.org/10.1016/j.jsg.2022.104723>
- 461 Natale, J., Vitale, S., Repola, L., Monti, L., & Isaia, R. (2023). Digital Surface Model Generated
462 from Vintage Aerial Photographs: a glance at the pre-urbanization morphology of the
463 active Campi Flegrei caldera. *Geomorphology*. Under review.
- 464 Nespoli, M., Tramelli, A., Belardinelli, M. E., & Bonafede, M. (2023). The effects of hot and
465 pressurized fluid flow across a brittle layer on the recent seismicity and deformation in the
466 Campi Flegrei caldera (Italy). *Journal of Volcanology and Geothermal Research*, 443,
467 107930.
- 468 Orsi, G., D'Antonio, M., de Vita, S., & Gallo, G. (1992). The Neapolitan Yellow Tuff, a large-
469 magnitude trachytic phreatoplinian eruption: eruptive dynamics, magma withdrawal and
470 caldera collapse. *Journal of Volcanology and Geothermal Research*, 53(1-4), 275-287.
- 471 Orsi, G., De Vita, S., & Di Vito, M. (1996). The restless, resurgent Campi Flegrei nested caldera
472 (Italy): constraints on its evolution and configuration. *Journal of Volcanology and*
473 *Geothermal Research*, 74(3-4), 179-214.
- 474 Orsi, G. (2022) Volcanic and Deformation History of the Campi Flegrei Volcanic Field, Italy in
475 Orsi, G., D'Antonio, M., Civetta, L. (Eds.), Campi Flegrei: A Restless Caldera in a Densely
476 Populated Area, Active Volcanoes of the World. Springer Berlin Heidelberg, Berlin,
477 Heidelberg. <https://doi.org/10.1007/978-3-642-37060-1>
- 478 Osservatorio Vesuviano, INGV (2023) Monthly Bulletin on Campi Flegrei,
- 479 Poupinet, G., Ellsworth, W. L., & Frechet, J. (1984). Monitoring velocity variations in the crust
480 using earthquake doublets: An application to the Calaveras Fault, California. *Journal of*

- 481 *Geophysical Research: Solid Earth*, 89(B7), 5719–5731.
482 <https://doi.org/10.1029/JB089iB07p05719>
- 483 Reasenber, P. A (1985) FPFIT, FPLOT, and FPPAGE : Fortran computer programs for
484 calculating and displaying earthquake fault-plane solutions, U.S. Geol. Surv. Open-File
485 Rep.,pp: 85-739
- 486 Richards-Dinger, K. B., & Shearer, P. M. (2000). Earthquake locations in southern California
487 obtained using source-specific station terms. *Journal of Geophysical Research: Solid*
488 *Earth*, 105(B5), 10939–10960. <https://doi.org/10.1029/2000JB900014>
- 489 Rosi, M., & Sbrana, A. (1987). Phlegrean fields. *Quaderni de la ricerca scientifica*, 9(114).
- 490 Sacchi, M., Pepe, F., Corradino, M., Insinga, D. D., Molisso, F., & Lubritto, C. (2014). The
491 Neapolitan Yellow Tuff caldera offshore the Campi Flegrei: Stratal architecture and
492 kinematic reconstruction during the last 15 ky. *Marine Geology*, 354, 15-33.
- 493 Scarpa, R. Bianco, F., Capuano, P. Castellano, M., D’Auria, L., Di Lieto, B. and Romano P. (2022)
494 Historic unrest of the Campi Flegrei Caldera, Italy in Orsi, G., D’Antonio, M., Civetta, L.
495 (Eds.), Campi Flegrei: A Restless Caldera in a Densely Populated Area, Active Volcanoes
496 of the World. Springer Berlin Heidelberg, Berlin, Heidelberg. [https://doi.org/10.1007/978-](https://doi.org/10.1007/978-3-642-37060-1)
497 [3-642-37060-1](https://doi.org/10.1007/978-3-642-37060-1)
- 498 Silleni, A., Giordano, G., Isaia, R., & Ort, M. H. (2020). The magnitude of the 39.8 ka Campanian
499 Ignimbrite eruption, Italy: method, uncertainties and errors. *Frontiers in Earth Science*, 8,
500 543399.
- 501 Steinmann, L., Spiess, V., & Sacchi, M. (2018). Post-collapse evolution of a coastal caldera
502 system: Insights from a 3D multichannel seismic survey from the Campi Flegrei caldera
503 (Italy). *Journal of Volcanology and Geothermal Research*, 349, 83-98.
- 504 Tamburello, G., Caliro, S., Chiodini, G., De Martino, P., Avino, R., Minopoli, C., Carandente, A.,
505 Rouwet, D., Aiuppa, A., Costa, A., Bitetto, M., Giudice, D., Francofonte, V., Ricci, T.,
506 Sciarra, A., Bagnato, E., & Capecchiacci, F. (2019). Escalating CO₂ degassing at the
507 Pisciarelli fumarolic system, and implications for the ongoing Campi Flegrei unrest.
508 *Journal of Volcanology and Geothermal Research*, 384, 151-157.
- 509 Tilling, R. I. (2008). The critical role of volcano monitoring in risk reduction. *Advances in*
510 *Geosciences*, 14, 3-11.

- 511 Todesco, M. (2021). Caldera's Breathing: Poroelastic Ground Deformation at Campi Flegrei
512 (Italy). *Frontiers in Earth Science* 9, 702665. <https://doi.org/10.3389/feart.2021.702665>
- 513 Tramelli, A., Giudicepietro, F., Ricciolino, P., & Chiodini, G. (2022). The seismicity of Campi
514 Flegrei in the contest of an evolving long term unrest. *Scientific reports*, 12(1), 2900.
- 515 Troiano, A., Isaia, R., Di Giuseppe, M. G., Tramparulo, F. D. A., & Vitale, S. (2019). Deep
516 Electrical Resistivity Tomography for a 3D picture of the most active sector of Campi
517 Flegrei caldera. *Scientific reports*, 9(1), 15124.
- 518 Troise, C., De Natale, G., Schiavone, R., Somma, R., & Moretti, R. (2019). The Campi Flegrei
519 caldera unrest: Discriminating magma intrusions from hydrothermal effects and
520 implications for possible evolution. *Earth-Science Reviews* 188, 108–122.
521 <https://doi.org/10.1016/j.earscirev.2018.11.007>
- 522 Young, N., Isaia, R., & Gottsmann, J. (2020). Gravimetric constraints on the hydrothermal system
523 of the Campi Flegrei caldera. *Journal of Geophysical Research: Solid Earth*, 125(7),
524 e2019JB019231.
- 525 Vanorio, T., J. Virieux, P. Capuano, & G. Russo (2005), Three-dimensional seismic tomography
526 from P wave and S wave microearthquake travel times and rock physics characterization
527 of the Campi Flegrei caldera. *Journal of Geophysical Research: Solid Earth*, 110, B03201,
528 doi:10.1029/2004JB003102.
- 529 Vanorio, T., & Kanitpanyacharoen, W. (2015). Rock physics of fibrous rocks akin to Roman
530 concrete explains uplifts at Campi Flegrei Caldera. *Science*, 349(6248), 617-621.
- 531 Vitale, S., Isaia, R., Ciarcia, S., Di Giuseppe, M. G., Iannuzzi, E., Prinzi, E. P., Tramparulo, F.D.A.,
532 & Troiano, A. (2019). Seismically induced soft-sediment deformation phenomena during
533 the volcano-tectonic activity of Campi Flegrei caldera (southern Italy) in the last 15 kyr.
534 *Tectonics*, 38(6), 1999-2018.
- 535 Vitale, S., & Natale, J. (2023). Combined volcano-tectonic processes for the drowning of the
536 Roman western coastal settlements at Campi Flegrei (southern Italy). *Earth Planets and*
537 *Space*, 75(1), 1-15.
- 538 Woo, J.Y.L., & Kilburn, C.R.J. (2010). Intrusion and deformation at Campi Flegrei, southern Italy:
539 Sills, dikes, and regional extension. *Journal of Geophysical Research: Solid Earth* 115,
540 2009JB006913. <https://doi.org/10.1029/2009JB006913>

541 Zollo, A., Judenherc, S., Auger, E., D’Auria, L., Virieux, J., Capuano, P., Chiarabba, C., De
542 Franco, R., Makris, J., Michelini, A., & Musacchio, G. (2003). Evidence for the buried rim
543 of Campi Flegrei caldera from 3-d active seismic imaging. *Geophysical Research Letters*
544 30, 2003GL018173. <https://doi.org/10.1029/2003GL018173>
545 Zollo, A., Maercklin, N., Vassallo, M., Dello Iacono, D., Virieux, J., & Gasparini, P. (2008),
546 Seismic reflections reveal a massive melt layer feeding Campi Flegrei caldera, *Geophysical*
547 *Research Letters* 35, L12306, doi:[10.1029/2008GL034242](https://doi.org/10.1029/2008GL034242).

548

549 **Open Research**

550 The phase arrival times used in this study are available at the INGV-Osservatorio Vesuviano
551 bulletin database, at the link <https://terremoti.ov.ingv.it/gossip/index.html>. Information is available
552 per event. Seismic waveforms can be accessed through EIDA portal (<https://eida.ingv.it/it/>),
553 network code IV. Relocated event catalog is available on zenodo at the link:
554 <https://doi.org/10.5281/zenodo.10259822> (Lomax and Scotto di Uccio, 2023). All earthquake
555 relocations were performed with NonLinLoc (Lomax et al., 2000; Lomax et al., 2014;
556 <http://www.alomax.net/nlloc>; <https://github.com/alomax/NonLinLoc>). SeismicityViewer
557 (<http://www.alomax.net/software>) was used for 3D seismicity analysis and plotting, ObsPy
558 (Krischer et al., 2015), (<http://obspy.org>) for waveform processing and coherence calculations.
559 NLL-SC processing parameters for the relocation of the seismicity are available on zenodo at the
560 link: <https://doi.org/10.5281/zenodo.10260849> (Lomax, 2023).

561

562 **Supporting Information summary**

563 Text S1 to S3

564 Figure S1 to S3

565 Table S1

566 Movie S1 to S3

567

568 **References in Supporting Information**

569 Brune, J. N. (1970). Tectonic stress and the spectra of seismic shear waves from earthquakes.
570 *Journal of Geophysical Research*, 75(26), 4997–5009.
571 <https://doi.org/10.1029/JB075i026p04997>

- 572 Keylis-Borok, V. (1959). On estimation of the displacement in an earthquake source and of source
573 dimensions. *Annals of Geophysics*, 12(2).
- 574 Judenherc, S., Zollo, A., 2004. The bay of Naples (southern Italy: Constraints on the volcanic
575 structures inferred from a dense seismic survey. *J. Geophys. Res. Solid Earth* 109 (B10).
576 <https://doi.org/10.1029/2003JB002876>.
- 577 Matoza, R. S., Shearer, P. M., Lin, G., Wolfe, C. J., & Okubo, P. G. (2013). Systematic relocation
578 of seismicity on Hawaii Island from 1992 to 2009 using waveform cross correlation and
579 cluster analysis. *Journal of Geophysical Research: Solid Earth*, 118(5), 2275-2288.
- 580 Podvin, P., & Lecomte, I. (1991). Finite difference computation of traveltimes in very contrasted
581 velocity models: a massively parallel approach and its associated tools. *Geophysical*
582 *Journal International*, 105(1), 271-284.
- 583 Reasenber, P. A. (1985). FPFIT, FPLOT, and FPPAGE: Fortran computer programs for
584 calculating and displaying earthquake fault-plane solutions. *US Geol. Surv. Open-File*
585 *Rep.*, 85-739.
- 586 Supino, M., Festa, G., & Zollo, A. (2019). A probabilistic method for the estimation of earthquake
587 source parameters from spectral inversion: Application to the 2016-2017 Central Italy
588 seismic sequence. *Geophysical Journal International*, 218(2), 988–1007.
589 <https://doi.org/10.1093/gji/ggz206>
- 590 Tarantola, A. (2004). *Inverse Problem Theory and Methods for Model Parameter Estimation*.
- 591 Tramelli, A., Godano, C., Ricciolino, P., Giudicepietro, F., Caliro, S., Orazi, M., ... & Chiodini,
592 G. (2021). Statistics of seismicity to investigate the Campi Flegrei caldera unrest. *Scientific*
593 *Reports*, 11(1), 7211.
- 594 Trugman, D. T., & Shearer, P. M. (2018). Strong correlation between stress drop and peak ground
595 acceleration for recent M 1–4 earthquakes in the San Francisco Bay area. *Bulletin of the*
596 *Seismological Society of America*, 108(2), 929-945.
- 597 Waldhauser, F., & Ellsworth, W. L. (2000). A double-difference earthquake location algorithm:
598 Method and application to the northern Hayward fault, California. *Bulletin of the*
599 *seismological society of America*, 90(6), 1353-1368.
- 600 Zhou, H. W. (1994). Rapid three-dimensional hypocentral determination using a master station
601 method. *Journal of Geophysical Research: Solid Earth*, 99(B8), 15439-15455.
- 602

1 **Delineation and Fine-Scale Structure of Active Fault Zones during**
2 **the 2014-2023 unrest at the Campi Flegrei Caldera (Southern Italy)**
3 **from High-Precision Earthquake Locations**

4
5 *Francesco Scotto di Uccio*¹, *Anthony Lomax*², *Jacopo Natale*³, *Titouan Muzellec*¹, *Gaetano*
6 *Festa*^{1,4}, *Sahar Nazeri*¹, *Vincenzo Convertito*⁵, *Antonella Bobbio*⁵, *Claudio Strumia*¹ and *Aldo*
7 *Zollo*¹

8
9 ¹ Department of Physics Ettore Pancini, Università di Napoli Federico II, Napoli, Italy

10 ² ALomax Scientific, Mouans-Sartoux, France

11 ³ Department of Earth and Geoenvironmental Sciences, Università di Bari “Aldo Moro”, Bari,
12 Italy

13 ⁴ Istituto Nazionale di Geofisica e Vulcanologia, Roma, Italy

14 ⁵ Osservatorio Vesuviano, Istituto Nazionale di Geofisica e Vulcanologia, Napoli, Italy

15 Corresponding author: Aldo Zollo (aldo.zollo@unina.it)

16
17 **Key Points:**

- 18 • High-precision location of 2014-2023 seismicity in Campi Flegrei images active fault
19 zones with unprecedented detail.
- 20 • From 2021 onwards the seismicity produces an elliptic pattern resembling that of the
21 1982-84 unrest phase of the caldera.
- 22 • Seismicity occurs along different volcano-tectonic structures including the inner ring
23 fault zone and faults bounding the Solfatara crater.

24 **Abstract**

25 In the past two decades, the central portion of Campi Flegrei caldera has experienced ground uplift
26 of up to 15 mm/month, and a consequent increase in the rate, magnitudes and extent of seismicity,
27 especially in the last two years. We use a new method for multi-scale precise earthquake location
28 to relocate the 2014-2023 seismicity and map in detail currently activated fault zones. We relate
29 the geometry, extent, and depth of these zones with available structural reconstructions of the
30 caldera. The current seismicity is mainly driven by the time-varying, ground-uplift induced stress
31 concentration on pre-existing, weaker fault zones, not only related to the inner caldera, dome
32 resurgence but also to ancient volcano-tectonic collapses and magma emplacement processes. The
33 extent of imaged fault segments suggests they can accommodate ruptures up to magnitude 5.0,
34 significantly increasing estimates of seismic hazard in the area.

35

36 **Plain Language Summary**

37 During the past two years, there has been a marked increase of ground uplift and number and size
38 of earthquakes at Campi Flegrei caldera. This increase in activity has raised concerns in the
39 population and public authorities about the impact of seismic activity on buildings and
40 infrastructure in the area and about the best actions to undertake during the seismic emergency to
41 reduce the risk. Additionally, the possibility of a future volcanic eruption is being considered,
42 although currently geochemical and geophysical monitoring shows no clear and unequivocal signs
43 of precursory phenomena. In this work we map the last decade of seismicity with high-precision
44 earthquake locations with the aim of unveiling the currently activated fault zones of the inner
45 caldera and assessing the potential hazard of earthquake ruptures along the delineated fault zone.
46 The results show an expanding, near-elliptical distribution of seismicity. The size of faults imaged
47 in the caldera suggest earthquakes up to magnitude 5.0 can occur, significantly increasing
48 estimates of seismic hazard in the area.

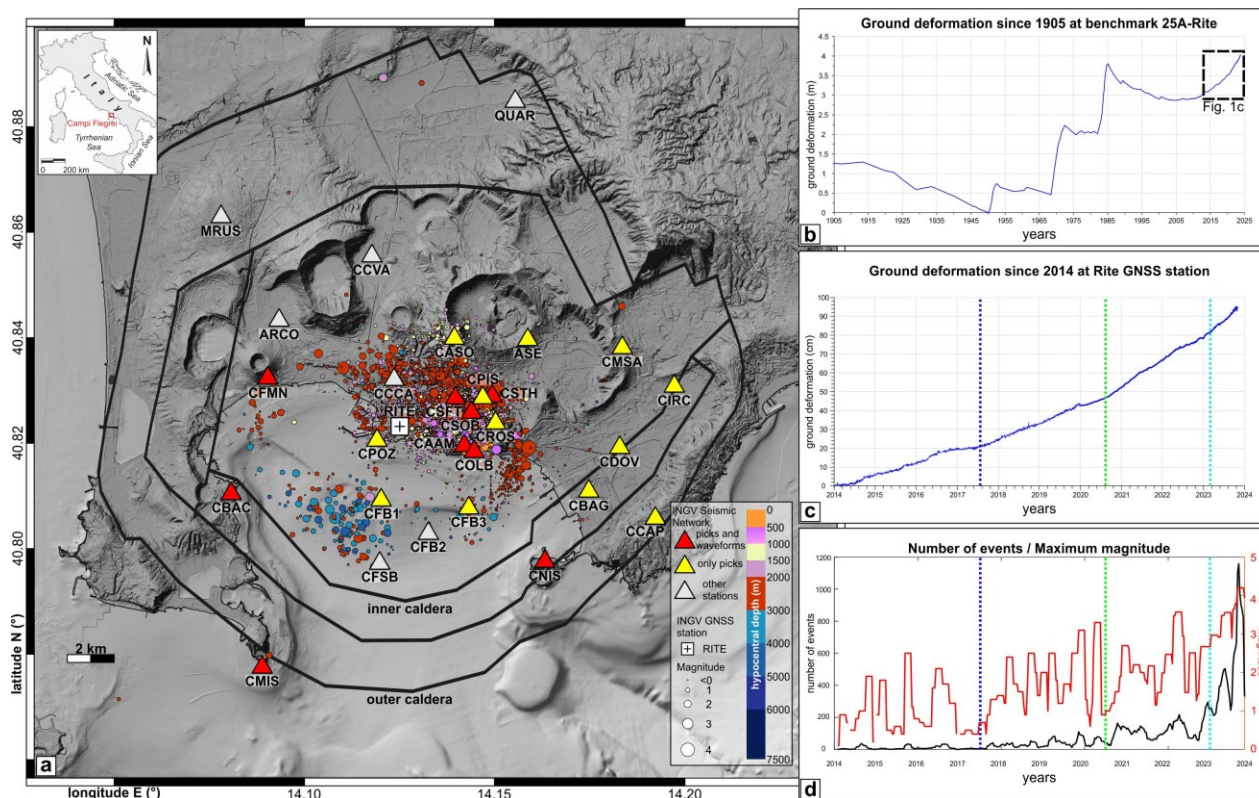
49

50 **1 Introduction**

51 The Campi Flegrei caldera, in Southern Italy is located nearby the one million people living in
52 wide metropolitan area of Napoli, making it the worldwide most densely urbanized volcanic area
53 (e.g., Charlton et al., 2020). During the past two decades, the central portion of Campi Flegrei
54 caldera experienced a sustained and continuous ground uplift, reaching rates of 15 mm/month,

55 with a consequent increase of the rate, magnitudes and extent of seismicity, especially in the last
 56 two years.

57



58

59 **Figure 1.** a) Shaded relief map of Campi Flegrei with simplified caldera boundaries (modified after Natale
 60 et al., 2022b), showing epicentral locations of the 2014-2023 seismicity recorded by INGV seismic network
 61 as retrieved from INGV-Osservatorio Vesuviano bulletin database
 62 (<https://terremoti.ov.ingv.it/gossip/index.html>), color coded by hypocentral depth and scaled by magnitude.
 63 Triangles show the location of seismic stations color-coded as follows: red for stations at which both picks
 64 and waveforms are available; yellow for stations with only picks available; gray for other INGV stations.
 65 White box with black cross shows the location of RITE GNSS station. b) Vertical ground deformation
 66 recorded at benchmark 25A and RITE GNSS station since 1905 (modified after Del Gaudio et al., 2010;
 67 INGV 2023 Monthly Bulletin), dashed black box shows the extent of Figure 1c. c) Uplift recorded at Rite
 68 GNSS station since 2014, vertical dotted lines indicate the occurrence of changes in uplift rate. d) Temporal
 69 evolution of number of events and maximum magnitude since 2014 computed in overlapping windows of
 70 60 days with a time shift of 10 days.

71

72 Extensive and accurate geophysical and geochemical monitoring is fundamental to understanding
 73 and modelling volcanic processes during unrest (Tilling, 2008). Changes in seismicity are usually

74 main precursors to volcanic eruptions, and are one of the primary indicators of the initiation and
75 evolution of a magmatic intrusion episode (McNutt et al., 1996). Since errors in earthquake
76 locations may preclude clear understanding of the ongoing processes, the use of precise seismicity
77 relocation techniques is emerging as a valuable tool to provide a comprehensive view of activated
78 faults and fractures during volcanic unrest, such as at the Campi Flegrei caldera.

79 The Campi Flegrei volcano is characterized by a nested caldera structure (Figure 1a; Orsi et al.,
80 1996; Orsi, 2022), produced by two large explosive eruptions, referred to as the Campanian
81 Ignimbrite (CI) and the Neapolitan Yellow Tuff (NYT), at 39 ka and 14.5 ka, respectively (Silleni
82 et al., 2020; Orsi et al., 1992), whose boundaries are now mapped also offshore (Natale et al.,
83 2022b). Since the NYT, over 70 eruptions occurred within the caldera boundaries, clustered in
84 time (i.e., volcanic epochs; Di Vito et al., 1999) and space along the main structural features (e.g.,
85 Bevilacqua et al., 2015). Since 10.5 ka, the volcanic activity is remarkably coupled with a caldera
86 resurgence phenomenon broadly acting in the central sector (Natale et al., 2022a), and displaying
87 a bell-shaped deformation pattern regardless of the scale and the polarity (uplift/subsidence). This
88 is similar to what is observed during historical ground deformation episodes (Bevilacqua et al.,
89 2020; Vitale and Natale, 2023).

90 Volcanic unrest and eruptions in the caldera are accompanied by seismotectonic phenomena.
91 Precursory seismicity and ground deformation patterns preceding the last historical eruption of
92 Monte Nuovo in 1538 CE (Di Vito et al., 2016) are similar to those in the current activity of the
93 caldera (Del Gaudio et al., 2010; Osservatorio Vesuviano – INGV, 2023).

94 Due to the high volcanic and seismic risk, the Campi Flegrei volcano hosts a highly advanced,
95 permanent multiparametric monitoring system (Bianco et al., 2022), including a dense seismic
96 monitoring network (Figure 1a). A series of ground uplift-subsidence with seismic activity
97 (bradyseismic) episodes affected the central area of Pozzuoli since early 1950s (Del Gaudio et al.,
98 2010), with the two most rapid uplift phases occurred in 1970-72 and 1982-84, reaching a
99 maximum uplift of about 4 m at RITE station in 1984 (Figure 1b), and producing over 20000
100 shallow earthquakes overall (D’Auria et al., 2011), concentrated in the Solfatara-Pisciarelli area
101 (Isaia et al., 2021). A long subsidence phase occurred between 1985 and 2005, with a maximum
102 subsidence of 90 cm and relatively rare seismicity (Gaeta et al., 2003). Since 2005 a new, long-
103 term, monotonic uplift phenomenon started with unsteadily accelerating seismicity (Bevilacqua et
104 al., 2022), especially from 2014 onwards (Figure 1c), which has produced a clear increase in the

105 number of seismic events and of the maximum magnitude (Figure 1d). At the beginning of 2023
106 the uplift surpassed the maximum elevation achieved during the previous 1982-1984 crisis (Figure
107 1b). The cause of the bradyseismic episodes is still debated within the volcanological community
108 (e.g., Troise et al., 2019). The main hypotheses are that the deformation is either directly caused
109 by pressure and/or volume changes induced by magma emplacement and intrusion at shallow
110 depths beneath the caldera (Woo and Kilburn, 2010; Macedonio et al., 2014) or it is due to the
111 poroelastic response of the shallow hydrothermal system to changes in pore pressure and fluid
112 content (Bonasia et al., 1984; Bonafede, 1991; Todesco, 2021; Nespoli et al., 2023). The latter
113 could be driven by the periodic migration toward the surface of crustal fluids possibly generated
114 by degassing processes at the primary, sill-like magma reservoir detected at 8 km depth by seismic
115 reflection experiments (Zollo et al., 2008). In favor of this second hypothesis, a lack of detectable
116 amount of magma at shallow depths was reported by previous seismic reflection soundings,
117 associated with the absence of univocal geochemical and geophysical magma movement signs
118 from multi-parametric data acquired by the dense monitoring system of the caldera (Vanorio et al.,
119 2005; Battaglia et al., 2008).

120 Changes in the deformation rate during the last ten years correlate with the changes in seismicity
121 rate and maximum magnitude of recorded events. Specifically, since 2020 there has been an
122 acceleration of ground uplift in the Campi Flegrei caldera, reaching in September 2023 a rate of
123 1-1.5 cm/month (Figures 1c, 1d), accompanied by an exponential increase in the earthquake rate
124 to about 1000 events per month (Figure 1d). Most of the earthquakes in the caldera occur at depths
125 shallower than 3 km, with a near-elliptical distribution as from the reference catalogue of INGV
126 (National Institute for Geophysics and Volcanology; Figure 1a). Most events have duration
127 magnitude $M_d \leq 1$, though starting in early 2023 there is a general increase of the average
128 magnitude per month, including several events with $M_d \geq 3$ and a largest, $M_d 4.2$ earthquake,
129 occurred on September 27, 2023.

130 The occurrence of five $M_d 3.6+$ earthquakes during the period August 18 – October 2, widely felt
131 in the Campi Flegrei and Napoli metropolitan area, raised a great concern in the population and
132 civil protection authorities about the earthquake risk related to the volcanic activity. Given the
133 high-density urbanization of the area, it is therefore important to understand the impact, including
134 potential damage, to buildings and infrastructures caused by the repeated occurrence of small to
135 moderate, shallow-depth events generated by the accelerating ground uplift.

136 In this study, we obtained multi-scale, high-precision relocations of the ongoing seismicity,
137 allowing to identify, with unprecedented detail, the location and geometry of the activated
138 structures during this crisis in the central area of the caldera. We used these new results along with
139 mapped surface faults and fractures and other geophysical information to better understand the
140 mechanics of earthquake faulting in relation to the caldera resurgence and other volcanic
141 phenomena, with the aim of identifying zones where future, larger magnitude earthquake can
142 potentially occur.

143

144 **2 Event Dataset**

145 We used P and S arrival-times from the earthquake catalogue provided by the INGV – Osservatorio
146 Vesuviano from 01/01/2014 to 14/11/2023 (Figure 1a), available at
147 <https://terremoti.ov.ingv.it/gossip/flegrei>. Phase arrivals and associated relative uncertainties and
148 event duration magnitudes M_d from only the fully located events in the catalogue (8292
149 earthquakes) are used. For the selected events, M_d ranges between -1.1 and 4.2, with the M_d 4.2
150 event (2023-09-27 01:35:34) having the largest number of phase arrival times (18 P and 6 S picks).
151 Events with lower magnitude ($M_d < 2$) typically show 6 to 10 P, 2 to 4 S arrival times. We also
152 extracted arrival times from 18 stations of the INGV national network (yellow and red triangles in
153 Figure 1a), located within 15 km from the catalogue epicentres. For the same set of events, we also
154 recovered vertical component waveforms from 9 velocimetric stations available on EIDA portal
155 (<https://eida.ingv.it>; red triangles in Figure 1a). We extracted waveforms in the time window from
156 10 s before to 45 s after the event origin time and decimated the traces to a sampling frequency of
157 50 Hz.

158

159 **3. High-precision earthquake location**

160 We obtained multi-scale, high-precision earthquake locations with a new procedure based on the
161 NonLinLoc location algorithm (Lomax et al., 2000; Lomax et al., 2014; NLL hereafter) which
162 produces an a-posterior probability density function (PDF) in 3D space for hypocentre location.
163 The new procedure, NLL-SSST-coherence (NLL-SC), combines source-specific, station travel-
164 time corrections (SSST) with stacking of PDFs, probabilistic location for nearby events based on
165 waveform similarity (Lomax and Savvaidis, 2022; Lomax and Henry, 2023).

166 In a first relocation step, NLL-SC iteratively develops SSST corrections on collapsing length scales

167 (Richards-Dinger and Shearer, 2000; Lomax and Savvaidis, 2022), which can greatly improve,
168 multi-scale relative location accuracy and clustering of events. In a second relocation step, NLL-
169 SC reduces finer scale relative errors by consolidating information across locations based on
170 waveform coherency between the events (Lomax and Savvaidis, 2022). This procedure is based
171 on the concept that if the waveforms for two events at a station are very similar (e.g., have high
172 coherency) up to a given frequency, then the distance between the two events is small relative to
173 the wavelength corresponding to that frequency (e.g., Geller and Mueller, 1980; Poupinet et al.,
174 1984). In this study we apply NLL-SC up to a frequency of 10 Hz, giving improved relative
175 location accuracy down to ~ 100 m scale. See the Supporting Information (Text S1) for more details
176 on the location procedure, velocity model (Figure S2) and processing parameters used in this study.
177

178 **4. Results**

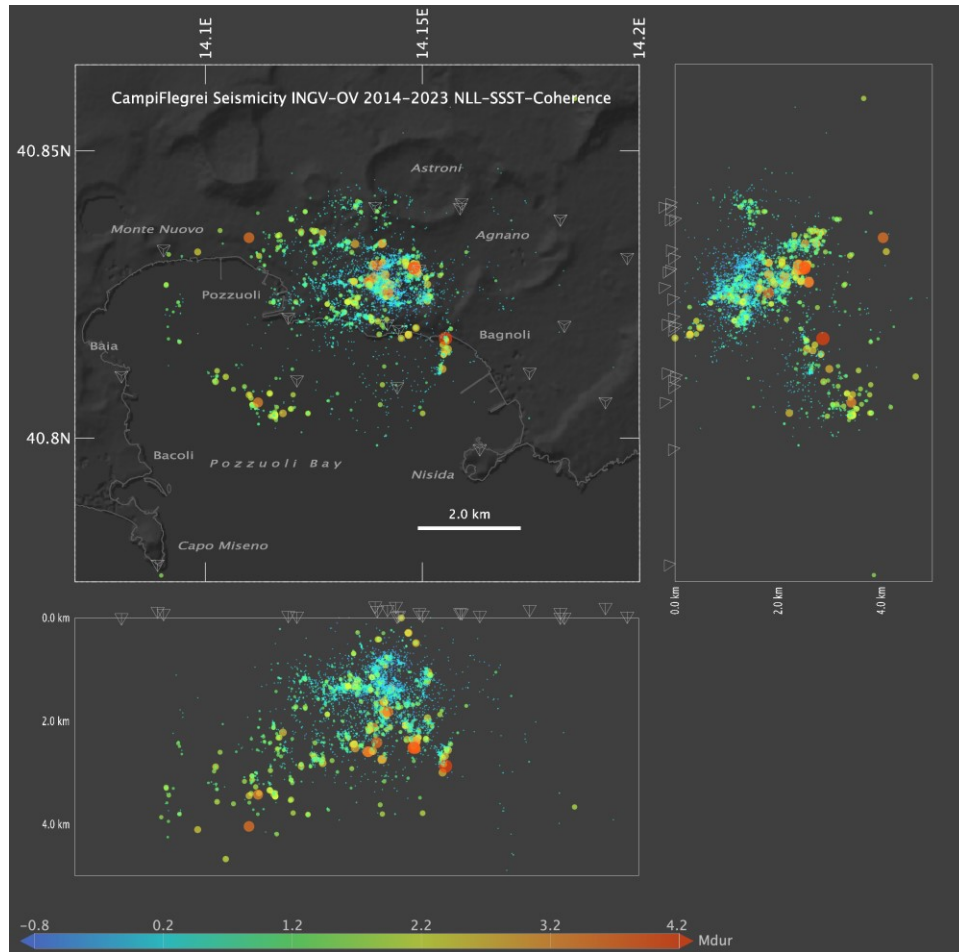
179 The high-precision NLL-SC locations delineate several clusters and alignments of seismicity
180 produced during the ongoing unrest at Campi Flegrei. Most of the seismicity concentrates in the
181 shallow region around the Solfatara-Pisciarelli area (cyan-green dots in Figure 2). Here, epicenters
182 define an $\sim 1 \times 1$ km, horseshoe-shaped structure, opened and deepening toward the northeast
183 beneath the Agnano Plain, and slightly larger than the ~ 0.5 km diameter of the Solfatara crater.
184 Smaller-scale seismicity clusters, with a typical size of 100-300m, occur south and southwest of
185 Solfatara, along the coast toward the center of Pozzuoli and the location of RITE station. This area
186 has been active since 2014 (Figure 3), although the seismicity has intensified during the last three
187 years.

188 The most recent magnitude $M_d 3.6+$ events, except for the largest magnitude $M_d 4.2$ earthquake,
189 also occurred in the Solfatara-Pisciarelli area, beneath the horseshoe-shaped seismicity, at depths
190 between 2 and 3.5 km. Northwest of the Solfatara crater, seismicity depicts a E-W trending, 1.5-
191 2.0 km long structure composed of event cluster at depths comparable to that of the major events
192 in the Solfatara.

193 Southeastward, off the coast of Bagnoli, a ~ 1 km long, sub-vertical alignment trending just E of N
194 is well defined by the relocated seismicity. This alignment contains the largest recorded event (M_d
195 4.2), which ruptured an area of $800-1200 \text{ m}^2$, according to the calculated source radius (Figure S1
196 of Supporting Information). Further offshore to the southwest the seismicity occurs at greater
197 depths, down to ~ 4 km, and forming a WNW oriented alignment offshore of Bacoli, and a N-S

198 alignment off the coast of Monte Nuovo. Overall, this seismicity forms an elliptical shape,
 199 punctuated by the lineations and clusters containing the larger magnitude ($M_d > 3$) events.

200



201

202 **Figure 2:** Relocated NLL-SC seismicity 2014-2023. Circles – color coded according to the magnitude
 203 duration - show earthquakes with duration magnitude $M_d \geq -1.0$ and ellipsoid major axis ≤ 2.0 km (7212
 204 of 8274 total relocated events); symbol size is proportional to magnitude. Tetrahedrons show subsets of
 205 stations from Figure 1a used for relocation.

206

207 The evolution of the seismicity over time (Figures 1d and 3) shows an increasing of the number of
 208 events and maximum magnitude. Moreover, while in the period 2014-2019 seismicity occurred at
 209 shallow depths (most of these events have depth < 2 km) and concentrated in the Solfatara-
 210 Pisciarelli area, during 2019-2023 the seismicity deepens, extends offshore and increases in
 211 maximum magnitude. During the last two years (2022-2023), the seismicity spreads to a larger
 212 area, forming the elliptical, ring-like structure, extending from inland north of Solfatara

213 southwards through Bagnoli, eastwards towards Bacoli and northward towards Monte Nuovo.

214

215 **5. Discussion**

216 The precisely located NLL-SC seismicity delineates the fault zones activated during the ongoing
217 seismic crisis at Campi Flegrei (Figure 2) with greater detail as compared to the raw bulletin dataset
218 (Figure 1a). Accurate delineation of the structures enables an improved interpretation of the fault
219 activation mechanisms in relation with the spatial stress variability and concentration as caused by
220 the extended ground uplift phenomenon. The multi-scale station corrections and waveform-
221 coherence based hypocenter consolidation of NLL-SC achieves a location precision of 100 m or
222 less, which is necessary to image faulting structures in a complex, multi-kilometer scale volcanic
223 environment such as Campi Flegrei.

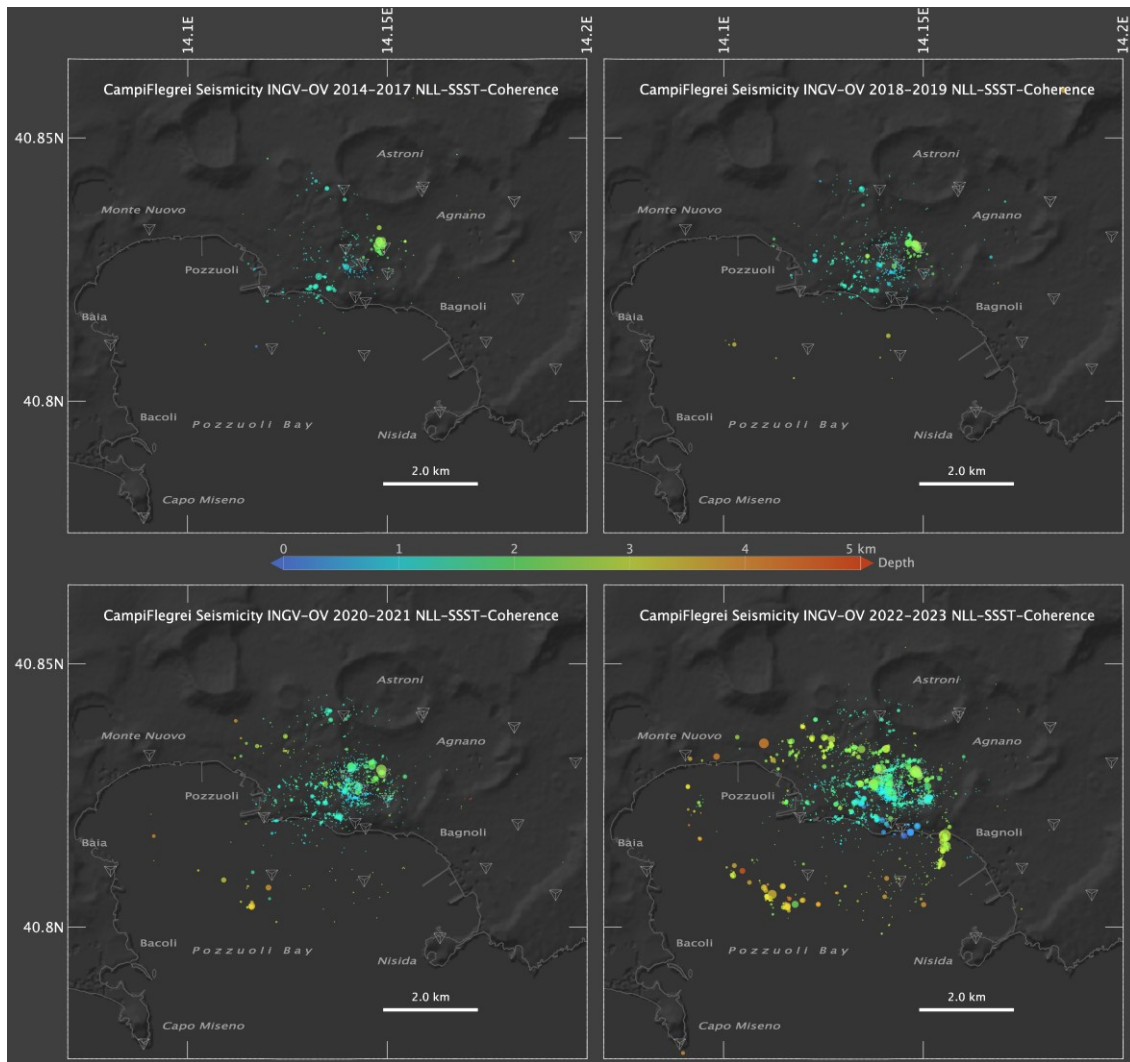
224 The spatiotemporal activation of shallow crustal volumes during 2014-2023 within the inner
225 caldera is shown by the relocated seismicity (Figure 3 and Supporting Information Video S1).

226 In the period 2014-2019 a low seismicity rate is observed (Figure 1c), mostly characterized by
227 small magnitude ($M_d < 2$) events occurring at depths shallower than about 3 km (Figure 3). These
228 events are located within a 1-2 km radius from the Solfatara crater which hosts, together with the
229 adjacent Pisciarelli fumarolic field, the most vigorous hydrothermal activity in the caldera
230 (Chiodini et al., 2017; Tamburello et al., 2019).

231 Overall, the variations in rate and magnitude of seismicity over time occur simultaneously with
232 changes in ground uplift rate of growth as observed at the station RITE in mid-2017, mid-2020
233 and end of 2022 (Figures 1c, d). Uplift velocity rather than cumulative uplift seems to control
234 localized seismicity production with the progressive activation of relatively long fracture zones at
235 the margin of the uplifting resurgent dome (Bevilacqua et al., 2022; Tramelli et al., 2022).

236 The spatial distribution of relocated seismicity (Figure 4) allows for an integrated geo-structural
237 interpretation based on recent evidence and reconstructions. The near-elliptical shape formed by
238 the seismicity since 2021 (Figure 4) resembles that of the 1982-84 crisis, whose seismicity
239 distribution has been related to a central collapsed portion of the caldera in studies (Barberi et al.,
240 1991; De Natale et al., 2006), which also considered results of gravity and magnetic surveys (Rosi
241 and Sbrana, 1987).

242



243
 244 **Figure 3:** Spatiotemporal evolution of the seismicity in periods 2014-2017, 2018-2019, 2020-2021 and
 245 2022-2023. Circles show earthquakes with magnitude $M_d \geq -1.0$ and ellipsoid major axis ≤ 2.0 km; symbol
 246 size is proportional to magnitude. Tetrahedrons show stations used for relocation.

247
 248 However, this hypothesis is contradicted by the geological evidence of a nested caldera structure
 249 (e.g., Orsi et al., 1996; Di Vito et al., 1999). Only a part of the relocated seismicity, occurring in
 250 the offshore sector (Feature A in Figure 4), is compatible with the caldera ring fault zone (e.g.,
 251 Sacchi et al., 2014; Steinmann et al., 2018). In a recent interpretation of high-resolution, seismic
 252 reflection profiles offshore of the caldera, Natale et al. (2022b) present evidence for a composite,
 253 ring-fault zone. This fault zone has an inner-ring confining from the west to the south-east the
 254 resurgent dome area, this latter being affected by a dense array of high-angle NE-SW to NNE-
 255 SSW trending, km-size collapse faults that cut the shallow marine sediments (Natale et al., 2020).

256 Several authors differentiate the inner-ring structure from the medial and outer ring fault systems,
257 whose expression at depth matches well the annular high-P-velocity, high-density body, imaged
258 by the 2001 active seismic tomography experiment and identified as the buried rim of the caldera
259 (Zollo et al., 2003; Judenherc and Zollo, 2004; Battaglia et al., 2008; Dello Iacono et al., 2009).
260 Only the deepest offshore seismicity, between 3-5 km depth, appears to fit and approximate the
261 downward propagation of the south-western inner ring fault (Figure 4a, f), where the most frequent
262 dip angles are between 60-80° (Natale et al., 2022b). This is consistent with a steep (~70°) inward-
263 dipping fault structure that justifies the 1.2 km spatial gap between the surface projection of the
264 mapped inner-ring fault and the 4 km deep epicenter locations. The focal mechanism solution (see
265 Supporting Information, Text S3) is consistent in terms of strike and dip of the nodal plane,
266 although with right-lateral kinematics (event 6 in Figure 4).

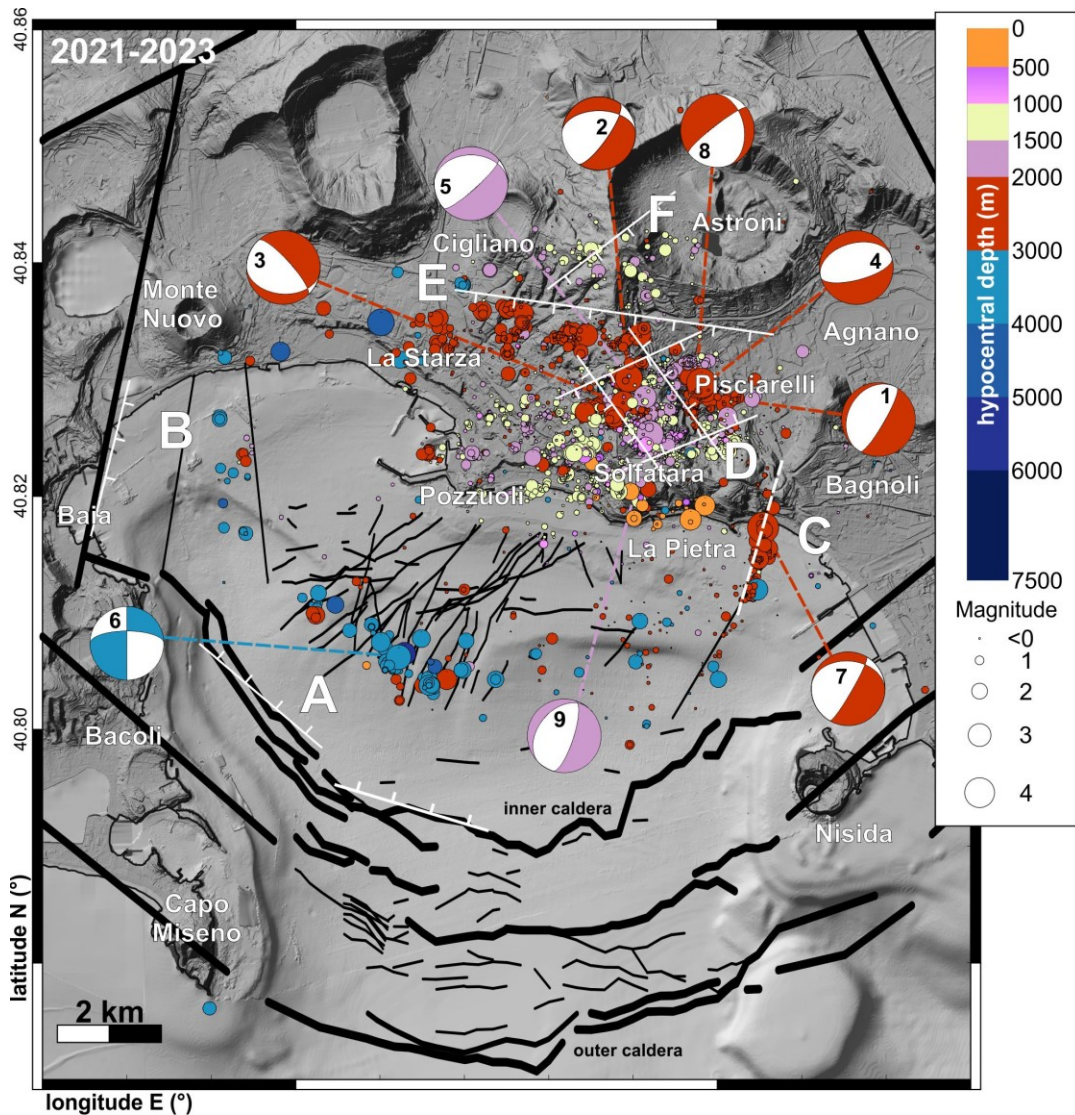
267 Activation of the Baia section (Feature B in Figure 4) of the inner ring fault (Vitale and Natale,
268 2023) can explain the seismicity off the coast of Monte Nuovo (between 3-5 km depth), where
269 underwater high-temperature hydrothermal manifestations occur (Di Napoli et al., 2016). The
270 more scattered and shallower seismicity could be related to high-angle faults as detailed in Natale
271 et al. (2022b), also involved by hot fluid uprise (Carlino et al., 2016).

272 Of particular interest is the near N-S trending sub-vertical fault structure just offshore La Pietra
273 (Feature C in Figure 4), generating the largest magnitude (Md 4.2) recorded event up to now during
274 the crisis, and overall producing earthquakes between 2-4 km depth. This structure has not been
275 identified previously as it lies in a region where no deep-penetrating seismic reflection profiles are
276 available. From spectral modelling of seismic displacement records the average seismic moment
277 and corner frequency of the event indicate a southward rupture extending over ~800-1200 m²
278 (Figure and Text S1 in Supporting Information), which is consistent with the area filled by nearby
279 seismicity (Figure 4), and the calculated focal mechanism (event 7 in Figure 4). However, given
280 the near-vertical dip angle and related hypocenter uncertainty, this fault structure could be dipping
281 to the east or to the west.

282 The offshore La Pietra fault structure illuminated by the relocated seismicity, represents a new
283 seismogenic feature in the caldera as compared to the 1982-84 crisis (e.g., Orsi et al., 1999). This
284 feature falls in the eastern portion of the near-elliptical seismicity pattern (Figure 4). The stress
285 drop estimated for the Md 4.2 event (2-3 MPa) in this structure is large in relation to the depth of

286 the structure, suggesting a high strength of rocks in the shallow caprock or underlying basement
 287 (Vanorio and Kanitpanyacharoen, 2015).

288



289 **Figure 4.** Simplified structural map showing the relationship between the epicentral distribution of
 290 relocated seismicity in the 2021-2023 period with the elliptical pattern and the main volcano-tectonic
 291 structures known in literature. Focal mechanisms solutions for selected 2023 $M_d > 3$ events are shown
 292 (details in Figure S3), with their color coded by depth.

294

295 Despite the moderate size of the event, the high stress drop acting over a small size asperity may
 296 be responsible for large peaks in the observed ground motion amplitudes (maximum recorded PGA
 297 of 0.3 g; see <http://shakemap.ingv.it/shake4/> archive.html).

298 In the Solfatara area (Figure 4, Feature D) the relocated seismicity matches well several fault arrays
299 mapped in the surface and subsurface geology. These fault arrays are related to the maar-diatreme
300 structure of Solfatara crater, whose polygonal shape is due to the presence of main NW-SE and
301 NE-SW faults, locally cross-cut by smaller E-W faults (Diamanti et al., 2022), and also exposed
302 at Pisciarelli fumarole field within the western rim of Agnano caldera (Isaia et al., 2021). Hence,
303 the horseshoe distribution of seismicity deepening eastward (Isaia et al., 2021) fits well the
304 presence of such array faults at depth, which significantly affects the hydrothermal circulation in
305 the area (Troiano et al., 2019). The calculated focal mechanisms (Figure 4 and Supporting
306 Information Text S3) show nodal planes consistent with the mapped structures, as they are mainly
307 NE-SW trending (events 1, 2, 5 and 8), and subordinately E-W trending (event 4) and NW-SE
308 (event 3).

309 An approximately E-W trending fault bounds the distribution of the relocated seismicity NE of the
310 Solfatara crater (Figure 4, Feature E), on which a series of spatially and temporally correlated
311 seismicity bursts occurred between 2 and 3 km depths. This structure corresponds to a south-
312 dipping normal fault with a left-lateral component, with noticeable surface expression in Agnano
313 and Cigliano as recently depicted in Natale et al. (2023) and corroborated by structural field data
314 by Diamanti et al. (2022). The bursts of seismicity occur along a ca. 6 km-long structure, that to
315 the west reaches La Starza marine terrace (Vitale et al., 2019), representing the northern border of
316 elliptical seismicity.

317 The NE-SW seismicity alignment (Figure 4, Feature F) in the Astroni might be associated with
318 pressurized fluids moving along a NE-SW faults within the shallow (1-1.5 km) portion of the
319 hydrothermal system (Isaia et al., 2022), where increased hydrothermal activity has been detected,
320 as corroborated by microgravity data (Young et al., 2020).

321

322 **5. Conclusions**

323 The general elliptical distribution of the ongoing seismicity at Campi Flegrei caldera is mainly
324 driven by the stress concentration causative effect of a bell-shaped ground deformation pattern
325 with fracture zones that appear coherent with the ones activated during the 1982-84 unrest in shape
326 and location (Scarpa et al., 2022). However, new sectors have been activated during the present
327 unrest, at the eastern boundary, where the largest Md 4.2 event was caused by a km-size rupture
328 within the shallow (3 km) volcanic sedimentary layer. We found that several structures delineated

329 by the ongoing seismicity have correspondence in the geological shallow fault record, whose
330 formation was not related to the same volcanic-tectonic process (i.e., dome resurgence), but rather
331 generated by other, more energetic processes such volcano-tectonic collapses, magma intrusion
332 and migration.

333 In general, the stress changes caused by the ongoing uplift of the central caldera appear to
334 concentrate on weaker pre-existing structures that are reactivated by small-to-moderate, sub-
335 kilometeric fractures. All the Md 3.6+ earthquake ruptures, apart from the largest Md 4.2 event,
336 have nucleated along segments of the complex SW-NE and SE-NW fault system array at the
337 margins of the Solfatara crater. As for the Md 4.2 event, the evidence for relatively high stress-
338 drops and average slip (2-3 MPa, 3-5 cm see Supporting Information) suggests a possible effect of
339 fluid-driven, pore-pressure increase at these faults that could favor the development of larger size
340 fractures.

341 Considering the size of the structures mapped in this study and the stress drop estimated for the
342 main event (Text S1 of Supporting Information), these faults can accommodate earthquakes of
343 moment magnitude up to 5.0, both beneath the Solfatara and offshore, south of Pozzuoli,
344 significantly increasing the hazard in the area.

345

346 **References**

- 347 Barberi, F., Cassano, E., La Torre, P., & Sbrana, A. (1991). Structural evolution of Campi Flegrei
348 caldera in light of volcanological and geophysical data. *Journal of volcanology and*
349 *geothermal research*, 48(1-2), 33-49.
- 350 Battaglia, J., Zollo, A., Virieux, J., & Dello Iacono, D. (2008). Merging active and passive data
351 sets in travelttime tomography: The case study of Campi Flegrei caldera (Southern Italy).
352 *Geophysical Prospecting*, 56, 555–573. <https://doi.org/10.1111/j.1365-2478.2007.00687.x>
- 353 Bevilacqua, A., Isaia, R., Neri, A., Vitale, S., Aspinall, W. P., Bisson, M., Flandoli, F., Baxter,
354 P.J., Bertagnini, A., Esposti Ongaro, T., Iannuzzi, E., Pistolesi, M., & Rosi, M. (2015).
355 Quantifying volcanic hazard at Campi Flegrei caldera (Italy) with uncertainty assessment:
356 1. Vent opening maps. *Journal of Geophysical Research: Solid Earth*, 120(4), 2309-2329.
- 357 Bevilacqua, A., Neri, A., De Martino, P., Isaia, R., Novellino, A., Tramparulo, F. D. A., & Vitale,
358 S. (2020). Radial interpolation of GPS and leveling data of ground deformation in a
359 resurgent caldera: application to Campi Flegrei (Italy). *Journal of Geodesy*, 94, 1-27.

- 360 Bevilacqua, A., De Martino, P., Giudicepietro, F., Ricciolino, P., Patra, A., Pitman, E. B., Bursik,
361 M., Voight, B., Flandoli, F., Macedonio, G., & Neri, A. (2022). Data analysis of the
362 unsteadily accelerating GPS and seismic records at Campi Flegrei caldera from 2000 to
363 2020. *Scientific reports*, 12(1), 19175.
- 364 Bianco, F., Caliro, S., De Martino, P., Orazi, M., Ricco, C., Vilardo, G., Aquino, I., Augusti, V.,
365 Avino, R., Bagnato, E., Brandi, G., Caputo, A., Carandente, A., Chiodini, G., Cuoco, E.,
366 D'Alessandro, A., Dolce, M., Guardato, S., Minopoli, C., Sansivro, F., Santi, A., Scarpato,
367 G., Tramelli, A., & Castellano, M. (2022). The permanent monitoring system of the Campi
368 Flegrei caldera, Italy. In *Campi Flegrei: A Restless Caldera in a Densely Populated Area*
369 (pp. 219-237). *Berlin, Heidelberg*. Springer Berlin Heidelberg.
- 370 Bonasia, V., Pingue, F., & Scarpa, R. (1984). A fluid-filled fracture as possible mechanism of
371 ground deformation at Phlegraean Fields, Italy, *Bullettin of Volcanology*, 47(2), 313–320.
- 372 Bonafede, M. (1991). Hot fluid migration: An efficient source of ground deformation: Application
373 to the 1982–1985 crisis at Campi Flegrei-Italy, *Journal of Volcanology and Geothermal*
374 *Research*, 48, 187–198.
- 375 Carlino, S., Mirabile, M., Troise, C., Sacchi, M., Zeni, L., Minardo, A., Caccavale, M., Daranyi,
376 V., & De Natale, G. (2016). Distributed-temperature-sensing using optical methods: a first
377 application in the offshore area of Campi Flegrei caldera (Southern Italy) for volcano
378 monitoring. *Remote Sensing*, 8(8), 674.
- 379 Charlton, D., Kilburn, C., & Edwards, S. (2020). Volcanic unrest scenarios and impact assessment
380 at Campi Flegrei caldera, Southern Italy. *Journal of Applied Volcanology*, 9, 1-26.
- 381 Chiodini, G., Selva, J., Del Pezzo, E., Marsan, D., De Siena, L., D'Auria, L., Bianco, F., Caliro,
382 S., De Martino, P., Ricciolino, P., & Petrillo, Z. (2017). Clues on the origin of post-2000
383 earthquakes at Campi Flegrei caldera (Italy). *Scientific reports*, 7(1), 4472.
- 384 De Natale, G., Troise, C., Pingue, F., Mastrolorenzo, G., Pappalardo, L., Battaglia, M., & Boschi,
385 E. (2006). The Campi Flegrei caldera: unrest mechanisms and hazards. *Geological Society,*
386 *London, Special Publications*, 269(1), 25-45.
- 387 Del Gaudio, C., Aquino, I., Ricciardi, G.P., Ricco, C., & Scandone, R. (2010). Unrest episodes at
388 Campi Flegrei: a reconstruction of vertical ground movements during 1905-2009. *Journal*
389 *of Volcanology and Geothermal Research*, 195, 48–56.

- 390 Dello Iacono, D., Zollo, A., Vassallo, M., Vanorio, T., & Judenherc, S. (2009). Seismic images
391 and rock properties of the very shallow structure of Campi Flegrei caldera (southern Italy).
392 *Bulletin of Volcanology* 71, 275–284. <https://doi.org/10.1007/s00445-008-0222-1>.
- 393 Diamanti, R., Camanni, G., Natale, J., & Vitale, S. (2022). A gravitational origin for volcano-
394 tectonic faults in the Campi Flegrei caldera (southern Italy) inferred from detailed field
395 observations. *Journal of Structural Geology*, 161, 104671.
- 396 Di Napoli, R., Aiuppa, A., Sulli, A., Caliro, S., Chiodini, G., Acocella, V., Ciraolo, G., Di Vito,
397 M. A., Interbartolo, F., Nasello, C., & Valenza, M. (2016). Hydrothermal fluid venting in
398 the offshore sector of Campi Flegrei caldera: A geochemical, geophysical, and
399 volcanological study. *Geochemistry, Geophysics, Geosystems*, 17(10), 4153-4178.
- 400 Di Vito, M. A., Isaia, R., Orsi, G., Southon, J. D., De Vita, S., d'Antonio, M., Pappalardo, L., &
401 Piochi, M. (1999). Volcanism and deformation since 12,000 years at the Campi Flegrei
402 caldera (Italy). *Journal of Volcanology and Geothermal Research*, 91(2–4), 221–246.
403 [https://doi.org/10.1016/S0377-0273\(99\)00037-2](https://doi.org/10.1016/S0377-0273(99)00037-2)
- 404 Di Vito, M. A., Acocella, V., Aiello, G., Barra, D., Battaglia, M., Carandente, A., Del Gaudio, C.,
405 de Vita, S., Ricciardi, G. P., Ricco, C., Scandone, R., & Terrasi, F. (2016). Magma transfer
406 at Campi Flegrei caldera (Italy) before the 1538 AD eruption, *Scientific Reports*, 6(1), 1–
407 9.
- 408 Gaeta, F. S., Peluso, F., Arienzo, I., Castagnolo, D., De Natale, G., Milano, G., Albanese, C. &
409 Mita, D. G. (2003). A physical appraisal of a new aspect of bradyseism: The miniuplifts.
410 *Journal of Geophysical Research: Solid Earth*, 108(B8).
- 411 Geller, R. J., & Mueller, C. S. (1980). Four similar earthquakes in central California. *Geophysical*
412 *Research Letters*, 7(10), 821–824. <https://doi.org/10.1029/GL007i010p00821>
- 413 Isaia, R., Di Giuseppe, M. G., Natale, J., Tramparulo, F. D. A., Troiano, A., & Vitale, S. (2021).
414 Volcano-tectonic setting of the Pisciarelli fumarole field, Campi Flegrei caldera, southern
415 Italy: Insights into fluid circulation patterns and hazard scenarios. *Tectonics*, 40(5),
416 e2020TC006227.
- 417 Isaia, R., Di Giuseppe, M. G., Troiano, A., Avino, R., Caliro, S., Santi, A., & Vitale, S. (2022).
418 Structure and present state of the Astroni Volcano in the Campi Flegrei caldera in Italy
419 based on multidisciplinary investigations. *Geochemistry Geophysics Geosystems*, 23(12),
420 e2022GC010534.

- 421 Judenherc, S., & Zollo, A. (2004). The Bay of Naples (southern Italy): Constraints on the volcanic
422 structures inferred from a dense seismic survey. *Journal of Geophysical Research: Solid*
423 *Earth*, 109(B10).
- 424 Krischer, L., Megies, T., Barsch, R., Beyreuther, M., Lecocq, T., Caudron, C., & Wassermann, J.
425 (2015). ObsPy: A bridge for seismology into the scientific Python ecosystem.
426 *Computational Science & Discovery*, 8(1), 014003.
- 427 Lomax, A., Virieux, J., Volant, P., & Berge-Thierry, C. (2000). Probabilistic Earthquake Location
428 in 3D and Layered Models. In C. H. Thurber & N. Rabinowitz (Eds.), *Advances in Seismic*
429 *Event Location*, 18, 101–134. Springer Netherlands. [https://doi.org/10.1007/978-94-015-](https://doi.org/10.1007/978-94-015-9536-0_5)
430 [9536-0_5](https://doi.org/10.1007/978-94-015-9536-0_5)
- 431 Lomax, A., Michelini, A., & Curtis, A. (2014). Earthquake Location, Direct, Global-Search
432 Methods. In R. A. Meyers (Ed.), *Encyclopedia of Complexity and Systems Science* (pp. 1–
433 33). Springer New York. https://doi.org/10.1007/978-3-642-27737-5_150-2
- 434 Lomax, A., & Savvaidis, A. (2022). High-Precision Earthquake Location Using Source-Specific
435 Station Terms and Inter-Event Waveform Similarity. *Journal of Geophysical Research:*
436 *Solid Earth*, 127(1), e2021JB023190. <https://doi.org/10.1029/2021JB023190>
- 437 Lomax, A., & Henry, P. (2023). Major California faults are smooth across multiple scales at
438 seismogenic depth. *Seismica*, 2(1), Article 1. <https://doi.org/10.26443/seismica.v2i1.324>.
- 439 Lomax, A., & Scotto di Uccio, F. (2023). Relocated event catalog for 2014-2023 seismicity at
440 Campi Flegrei [Data set]. *Zenodo*. <https://doi.org/10.5281/zenodo.10259822>
- 441 Lomax, A. (2023). NLL-SC processing parameters for the relocation of the 2014-2023 Campi
442 Flegrei seismicity [Data set]. *Zenodo*. <https://doi.org/10.5281/zenodo.10260849>
- 443 Macedonio, G., Giudicepietro, F., D’Auria, L., & Martini, M. (2014). Sill intrusion as a source
444 mechanism of unrest at volcanic calderas. *Journal of Geophysical Research: Solid Earth*,
445 119, 3986–4000. <https://doi.org/10.1002/2013JB010868>
- 446 McNutt, S. R., Scarpa, R., & Tilling, R. I. (1996). Monitoring and mitigation of volcano hazards.
447 In *Berlin, Federal Republic of Germany, Springer-Verlag, Ch. Seismic monitoring and*
448 *eruption forecasting of volcanoes: a review of the state-of-the-art and case histories* (pp.
449 99-146)

- 450 Natale, J., Ferranti, L., Marino, C., & Sacchi, M. (2020). Resurgent dome faults in the offshore of
451 the Campi Flegrei caldera (Pozzuoli Bay, Campania): preliminary results from high-
452 resolution seismic reflection profiles. *Bollettino di Geofisica Teorica ed Applicata*, 61(3).
- 453 Natale, J., Ferranti, L., Isaia, R., Marino, C., Sacchi, M., Spiess, V., Steinmann, L., & Vitale, S.
454 (2022a). Integrated on-land-offshore stratigraphy of the Campi Flegrei caldera: new
455 insights into the volcano-tectonic evolution in the last 15 kyr. *Basin Research* 34 (2), 855–
456 882.
- 457 Natale, J., Camanni, G., Ferranti, L., Isaia, R., Sacchi, M., Spiess, V., Steinmann, L., & Vitale, S.
458 (2022b). Fault systems in the offshore sector of the Campi Flegrei caldera (southern Italy):
459 implications for nested caldera structure, resurgent dome, and volcano-tectonic evolution.
460 *Journal of Structural Geology*. 163:104723. <https://doi.org/10.1016/j.jsg.2022.104723>
- 461 Natale, J., Vitale, S., Repola, L., Monti, L., & Isaia, R. (2023). Digital Surface Model Generated
462 from Vintage Aerial Photographs: a glance at the pre-urbanization morphology of the
463 active Campi Flegrei caldera. *Geomorphology*. *Under review*.
- 464 Nespoli, M., Tramelli, A., Belardinelli, M. E., & Bonafede, M. (2023). The effects of hot and
465 pressurized fluid flow across a brittle layer on the recent seismicity and deformation in the
466 Campi Flegrei caldera (Italy). *Journal of Volcanology and Geothermal Research*, 443,
467 107930.
- 468 Orsi, G., D'Antonio, M., de Vita, S., & Gallo, G. (1992). The Neapolitan Yellow Tuff, a large-
469 magnitude trachytic phreatoplinian eruption: eruptive dynamics, magma withdrawal and
470 caldera collapse. *Journal of Volcanology and Geothermal Research*, 53(1-4), 275-287.
- 471 Orsi, G., De Vita, S., & Di Vito, M. (1996). The restless, resurgent Campi Flegrei nested caldera
472 (Italy): constraints on its evolution and configuration. *Journal of Volcanology and*
473 *Geothermal Research*, 74(3-4), 179-214.
- 474 Orsi, G. (2022) Volcanic and Deformation History of the Campi Flegrei Volcanic Field, Italy in
475 Orsi, G., D'Antonio, M., Civetta, L. (Eds.), Campi Flegrei: A Restless Caldera in a Densely
476 Populated Area, Active Volcanoes of the World. Springer Berlin Heidelberg, Berlin,
477 Heidelberg. <https://doi.org/10.1007/978-3-642-37060-1>
- 478 Osservatorio Vesuviano, INGV (2023) Monthly Bulletin on Campi Flegrei,
- 479 Poupinet, G., Ellsworth, W. L., & Frechet, J. (1984). Monitoring velocity variations in the crust
480 using earthquake doublets: An application to the Calaveras Fault, California. *Journal of*

- 481 *Geophysical Research: Solid Earth*, 89(B7), 5719–5731.
482 <https://doi.org/10.1029/JB089iB07p05719>
- 483 Reasenber, P. A (1985) FPFIT, FPLOT, and FPPAGE : Fortran computer programs for
484 calculating and displaying earthquake fault-plane solutions, U.S. Geol. Surv. Open-File
485 Rep.,pp: 85-739
- 486 Richards-Dinger, K. B., & Shearer, P. M. (2000). Earthquake locations in southern California
487 obtained using source-specific station terms. *Journal of Geophysical Research: Solid*
488 *Earth*, 105(B5), 10939–10960. <https://doi.org/10.1029/2000JB900014>
- 489 Rosi, M., & Sbrana, A. (1987). Phlegrean fields. *Quaderni de la ricerca scientifica*, 9(114).
- 490 Sacchi, M., Pepe, F., Corradino, M., Insinga, D. D., Molisso, F., & Lubritto, C. (2014). The
491 Neapolitan Yellow Tuff caldera offshore the Campi Flegrei: Stratal architecture and
492 kinematic reconstruction during the last 15 ky. *Marine Geology*, 354, 15-33.
- 493 Scarpa, R., Bianco, F., Capuano, P., Castellano, M., D’Auria, L., Di Lieto, B. and Romano P. (2022)
494 Historic unrest of the Campi Flegrei Caldera, Italy in Orsi, G., D’Antonio, M., Civetta, L.
495 (Eds.), Campi Flegrei: A Restless Caldera in a Densely Populated Area, Active Volcanoes
496 of the World. Springer Berlin Heidelberg, Berlin, Heidelberg. [https://doi.org/10.1007/978-](https://doi.org/10.1007/978-3-642-37060-1)
497 [3-642-37060-1](https://doi.org/10.1007/978-3-642-37060-1)
- 498 Silleni, A., Giordano, G., Isaia, R., & Ort, M. H. (2020). The magnitude of the 39.8 ka Campanian
499 Ignimbrite eruption, Italy: method, uncertainties and errors. *Frontiers in Earth Science*, 8,
500 543399.
- 501 Steinmann, L., Spiess, V., & Sacchi, M. (2018). Post-collapse evolution of a coastal caldera
502 system: Insights from a 3D multichannel seismic survey from the Campi Flegrei caldera
503 (Italy). *Journal of Volcanology and Geothermal Research*, 349, 83-98.
- 504 Tamburello, G., Caliro, S., Chiodini, G., De Martino, P., Avino, R., Minopoli, C., Carandente, A.,
505 Rouwet, D., Aiuppa, A., Costa, A., Bitetto, M., Giudice, D., Francofonte, V., Ricci, T.,
506 Sciarra, A., Bagnato, E., & Capecchiacci, F. (2019). Escalating CO₂ degassing at the
507 Pisciarelli fumarolic system, and implications for the ongoing Campi Flegrei unrest.
508 *Journal of Volcanology and Geothermal Research*, 384, 151-157.
- 509 Tilling, R. I. (2008). The critical role of volcano monitoring in risk reduction. *Advances in*
510 *Geosciences*, 14, 3-11.

- 511 Todesco, M. (2021). Caldera's Breathing: Poroelastic Ground Deformation at Campi Flegrei
512 (Italy). *Frontiers in Earth Science* 9, 702665. <https://doi.org/10.3389/feart.2021.702665>
- 513 Tramelli, A., Giudicepietro, F., Ricciolino, P., & Chiodini, G. (2022). The seismicity of Campi
514 Flegrei in the contest of an evolving long term unrest. *Scientific reports*, 12(1), 2900.
- 515 Troiano, A., Isaia, R., Di Giuseppe, M. G., Tramparulo, F. D. A., & Vitale, S. (2019). Deep
516 Electrical Resistivity Tomography for a 3D picture of the most active sector of Campi
517 Flegrei caldera. *Scientific reports*, 9(1), 15124.
- 518 Troise, C., De Natale, G., Schiavone, R., Somma, R., & Moretti, R. (2019). The Campi Flegrei
519 caldera unrest: Discriminating magma intrusions from hydrothermal effects and
520 implications for possible evolution. *Earth-Science Reviews* 188, 108–122.
521 <https://doi.org/10.1016/j.earscirev.2018.11.007>
- 522 Young, N., Isaia, R., & Gottsmann, J. (2020). Gravimetric constraints on the hydrothermal system
523 of the Campi Flegrei caldera. *Journal of Geophysical Research: Solid Earth*, 125(7),
524 e2019JB019231.
- 525 Vanorio, T., J. Virieux, P. Capuano, & G. Russo (2005), Three-dimensional seismic tomography
526 from P wave and S wave microearthquake travel times and rock physics characterization
527 of the Campi Flegrei caldera. *Journal of Geophysical Research: Solid Earth*, 110, B03201,
528 doi:10.1029/2004JB003102.
- 529 Vanorio, T., & Kanitpanyacharoen, W. (2015). Rock physics of fibrous rocks akin to Roman
530 concrete explains uplifts at Campi Flegrei Caldera. *Science*, 349(6248), 617-621.
- 531 Vitale, S., Isaia, R., Ciarcia, S., Di Giuseppe, M. G., Iannuzzi, E., Prinzi, E. P., Tramparulo, F.D.A.,
532 & Troiano, A. (2019). Seismically induced soft-sediment deformation phenomena during
533 the volcano-tectonic activity of Campi Flegrei caldera (southern Italy) in the last 15 kyr.
534 *Tectonics*, 38(6), 1999-2018.
- 535 Vitale, S., & Natale, J. (2023). Combined volcano-tectonic processes for the drowning of the
536 Roman western coastal settlements at Campi Flegrei (southern Italy). *Earth Planets and*
537 *Space*, 75(1), 1-15.
- 538 Woo, J.Y.L., & Kilburn, C.R.J. (2010). Intrusion and deformation at Campi Flegrei, southern Italy:
539 Sills, dikes, and regional extension. *Journal of Geophysical Research: Solid Earth* 115,
540 2009JB006913. <https://doi.org/10.1029/2009JB006913>

541 Zollo, A., Judenherc, S., Auger, E., D’Auria, L., Virieux, J., Capuano, P., Chiarabba, C., De
542 Franco, R., Makris, J., Michelini, A., & Musacchio, G. (2003). Evidence for the buried rim
543 of Campi Flegrei caldera from 3-d active seismic imaging. *Geophysical Research Letters*
544 30, 2003GL018173. <https://doi.org/10.1029/2003GL018173>
545 Zollo, A., Maercklin, N., Vassallo, M., Dello Iacono, D., Virieux, J., & Gasparini, P. (2008),
546 Seismic reflections reveal a massive melt layer feeding Campi Flegrei caldera, *Geophysical*
547 *Research Letters* 35, L12306, doi:[10.1029/2008GL034242](https://doi.org/10.1029/2008GL034242).

548

549 **Open Research**

550 The phase arrival times used in this study are available at the INGV-Osservatorio Vesuviano
551 bulletin database, at the link <https://terremoti.ov.ingv.it/gossip/index.html>. Information is available
552 per event. Seismic waveforms can be accessed through EIDA portal (<https://eida.ingv.it/it/>),
553 network code IV. Relocated event catalog is available on zenodo at the link:
554 <https://doi.org/10.5281/zenodo.10259822> (Lomax and Scotto di Uccio, 2023). All earthquake
555 relocations were performed with NonLinLoc (Lomax et al., 2000; Lomax et al., 2014;
556 <http://www.alomax.net/nlloc>; <https://github.com/alomax/NonLinLoc>). SeismicityViewer
557 (<http://www.alomax.net/software>) was used for 3D seismicity analysis and plotting, ObsPy
558 (Krischer et al., 2015), (<http://obspy.org>) for waveform processing and coherence calculations.
559 NLL-SC processing parameters for the relocation of the seismicity are available on zenodo at the
560 link: <https://doi.org/10.5281/zenodo.10260849> (Lomax, 2023).

561

562 **Supporting Information summary**

563 Text S1 to S3

564 Figure S1 to S3

565 Table S1

566 Movie S1 to S3

567

568 **References in Supporting Information**

569 Brune, J. N. (1970). Tectonic stress and the spectra of seismic shear waves from earthquakes.
570 *Journal of Geophysical Research*, 75(26), 4997–5009.
571 <https://doi.org/10.1029/JB075i026p04997>

- 572 Keylis-Borok, V. (1959). On estimation of the displacement in an earthquake source and of source
573 dimensions. *Annals of Geophysics*, 12(2).
- 574 Judenherc, S., Zollo, A., 2004. The bay of Naples (southern Italy: Constraints on the volcanic
575 structures inferred from a dense seismic survey. *J. Geophys. Res. Solid Earth* 109 (B10).
576 <https://doi.org/10.1029/2003JB002876>.
- 577 Matoza, R. S., Shearer, P. M., Lin, G., Wolfe, C. J., & Okubo, P. G. (2013). Systematic relocation
578 of seismicity on Hawaii Island from 1992 to 2009 using waveform cross correlation and
579 cluster analysis. *Journal of Geophysical Research: Solid Earth*, 118(5), 2275-2288.
- 580 Podvin, P., & Lecomte, I. (1991). Finite difference computation of traveltimes in very contrasted
581 velocity models: a massively parallel approach and its associated tools. *Geophysical*
582 *Journal International*, 105(1), 271-284.
- 583 Reasenber, P. A. (1985). FPFIT, FPLOT, and FPPAGE: Fortran computer programs for
584 calculating and displaying earthquake fault-plane solutions. *US Geol. Surv. Open-File*
585 *Rep.*, 85-739.
- 586 Supino, M., Festa, G., & Zollo, A. (2019). A probabilistic method for the estimation of earthquake
587 source parameters from spectral inversion: Application to the 2016-2017 Central Italy
588 seismic sequence. *Geophysical Journal International*, 218(2), 988–1007.
589 <https://doi.org/10.1093/gji/ggz206>
- 590 Tarantola, A. (2004). *Inverse Problem Theory and Methods for Model Parameter Estimation*.
- 591 Tramelli, A., Godano, C., Ricciolino, P., Giudicepietro, F., Caliro, S., Orazi, M., ... & Chiodini,
592 G. (2021). Statistics of seismicity to investigate the Campi Flegrei caldera unrest. *Scientific*
593 *Reports*, 11(1), 7211.
- 594 Trugman, D. T., & Shearer, P. M. (2018). Strong correlation between stress drop and peak ground
595 acceleration for recent M 1–4 earthquakes in the San Francisco Bay area. *Bulletin of the*
596 *Seismological Society of America*, 108(2), 929-945.
- 597 Waldhauser, F., & Ellsworth, W. L. (2000). A double-difference earthquake location algorithm:
598 Method and application to the northern Hayward fault, California. *Bulletin of the*
599 *seismological society of America*, 90(6), 1353-1368.
- 600 Zhou, H. W. (1994). Rapid three-dimensional hypocentral determination using a master station
601 method. *Journal of Geophysical Research: Solid Earth*, 99(B8), 15439-15455.
- 602

1 Supporting Information for

2 **Delineation and Fine-Scale Structure of Active Fault Zones during**
3 **the 2014-2023 unrest at the Campi Flegrei Caldera (Southern Italy)**
4 **from High-Precision Earthquake Locations**

5
6 *Francesco Scotto di Uccio*¹, *Anthony Lomax*², *Jacopo Natale*³, *Titouan Muzellec*¹, *Gaetano*
7 *Festa*^{1,4}, *Sahar Nazeri*¹, *Vincenzo Convertito*⁵, *Antonella Bobbio*⁵, *Claudio Strumia*¹ and *Aldo*
8 *Zollo*¹

9
10 ¹ Department of Physics Ettore Pancini, Università di Napoli Federico II, Napoli, Italy

11 ² ALomax Scientific, Mouans-Sartoux, France

12 ³ Department of Earth and Geoenvironmental Sciences, Università di Bari “Aldo Moro”, Bari,
13 Italy

14 ⁴ Istituto Nazionale di Geofisica e Vulcanologia, Roma, Italy

15 ⁵ Osservatorio Vesuviano, Istituto Nazionale di Geofisica e Vulcanologia, Napoli, Italy

16
17 Corresponding author: Aldo Zollo (aldo.zollo@unina.it)

18
19 **Contents of this file**

20 Text from S1 to S3

21 Figure S1 to S2

22 Table S1

23
24 **Additional Supporting Information (Files uploaded separately)**

25 Captions for Movie S1 to S3

26
27 **Introduction**

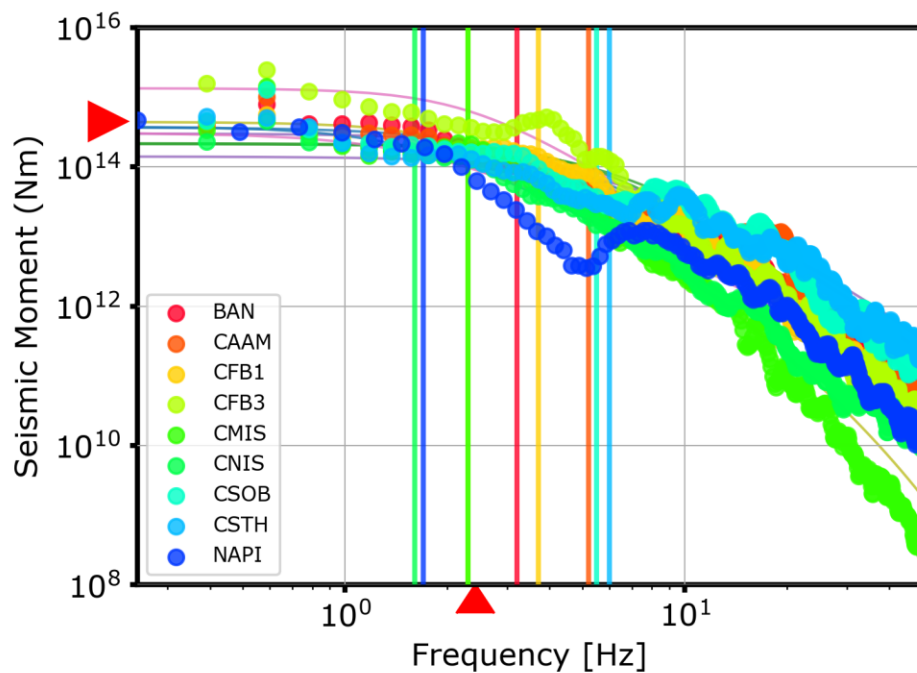
28 In the Supplementary information, we present the estimation of the source parameters for the main
29 event (M_d 4.2) from spectral modelling (Text S1), the details of the location technique, that has
30 been applied to the 2014-2023 Campi Flegrei arrival times and waveforms (Text S2) and the
31 estimation of the focal mechanisms for the main events ($M_d > 3.0$) in the catalogue (Text S3).

32

33 **Text S1: Source parameters for the main event**

34 For the main event in the dataset (M_d 4.2) occurred on the 2023/09/27 01:35:34 we analyzed
35 source parameters from frequency domain inversion of S-wave amplitude spectra. The inversion
36 follows the approach proposed by Supino et al. (2019), where a generalized Brune's model (Brune,
37 1970) is used to evaluate source parameters and their associated uncertainties based on integration
38 of the a posteriori Probability Density Function (PDF) (Tarantola, 2004).

39



40

41 **Figure S1:** Spectral amplitudes (circles) and of spectral amplitudes fits (lines) with color code representing
42 the different stations. Vertical lines mark corner frequency estimations at single stations, while red arrows
43 indicate the final estimation of Seismic moment M_0 and corner frequency f_c for the event.

44

45 For the analysis the displacement amplitude spectra recorded at available nearby stations (red
46 triangles in Figure 1) were used after removal of the instrumental response. Manual picking of the
47 event allowed to select 3s time windows around the S wave (0.2s before and 2.8 after the pick) to

48 be used for the inversion. Anelastic attenuation was taken into account by considering a constant
49 quality factor $Q = 150$, while the wave propagation velocity was fixed to $v_s = 3000\text{m/s}$ with
50 density $\rho = 2.5\text{g/cm}^3$ (Judenherc and Zollo, 2004). Spectral fit is shown in Figure S1.

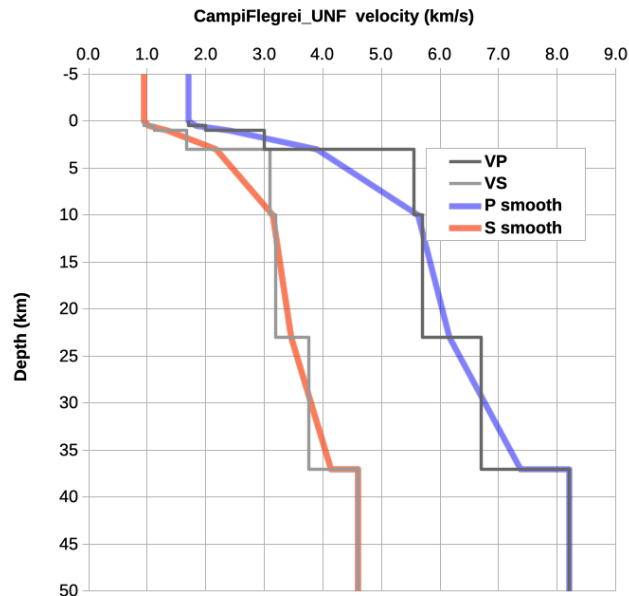
51 The moment magnitude was estimated to be $M_w = 3.68 \pm 0.02$ with corner frequency $f_c = 2.4 \pm$
52 0.1 Hz . The stress drop from Kelis-Borok (1959) relation results $\Delta\sigma = 2.3 \pm 0.5\text{ MPa}$. Finally,
53 the retrieved source radius $a = 460 \pm 20\text{ m}$ suggests that the rupture process involved a fault with
54 a length of about 1 km . The average slip was estimated to be of the order of 3-5 cm.

55

56 **Text S2: High-precision earthquake relocation procedures**

57 *General framework*

58 We obtain multi-scale high-precision earthquake relocations with NLL-SSST-coherence, which
59 combines of source-specific, station traveltime corrections (SSST) and stacking of probabilistic
60 locations for nearby event based on inter-event waveform coherence (Lomax and Savvaidis, 2022;
61 Lomax and Henry, 2023). These procedures are extensions of the NonLinLoc location algorithm
62 (Lomax et al., 2000, Lomax et al. 2014; NLL hereafter), which performs efficient, global sampling
63 to generate a posterior probability density function (PDF) in 3D space for hypocenter location.
64 This PDF provides a comprehensive description of likely hypocentral locations and their
65 uncertainty, and enables application of the waveform coherence relocation. Within NLL, we used
66 the equal differential-timing (EDT) likelihood function (Zhou, 1994; Lomax et al., 2014), which
67 is highly robust in the presence of outlier data caused by large error in phase identification,
68 measured arrival-times or predicted traveltimes. We use a finite-differences, eikonal-equation
69 algorithm (Podvin and Lecomte, 1991) to calculate gridded P and S traveltimes for initial NLL
70 locations using a smoothed version (Figure S2) of the velocity model used by the seismic
71 laboratory from INGV-Osservatorio Vesuviano (Tramelli et al., 2021).



72

73 **Figure S2:** Smoothed P and S velocity model, drawn from the velocity model used by the seismic laboratory
 74 at INGV-Osservatorio Vesuviano (Tramelli et al., 2021).

75

76 *Source-specific station term corrections*

77 In a first relocation stage, NLL-SSST-coherence iteratively develops SSST corrections on
 78 collapsing length scales (Richards-Dinger and Shearer, 2000; Lomax and Savvaidis, 2022), which
 79 can greatly improve, multi-scale, relative location accuracy and clustering of events. In contrast
 80 to station static corrections, which give a unique time correction for each station and phase type,
 81 SSST corrections vary smoothly throughout a 3D volume to specify a source-position dependent
 82 correction for each station and phase type. These corrections account for 3D variations in velocity
 83 structure and corresponding distortion in source-receiver ray paths. Spatial-varying, SSST
 84 corrections are most effective for improving relative locations on all scales when the ray paths
 85 between stations and events differ greatly across the studied seismicity. SSST corrections can
 86 improve multi-scale precision when epistemic error in the velocity model is large, such as when a
 87 1D, laterally homogeneous model or a large-wavelength, smooth model is used in an area with
 88 sharp, lateral velocity contrasts or smaller scale, 3D heterogeneities.

89 *Waveform coherency relocation*

90 In a second relocation stage, NLL-SSST-coherence reduces aleatoric location error by
91 consolidating information across event locations based on waveform coherency between the events
92 (Lomax and Savvaidis, 2022). This coherency relocation, NLL-coherence, is based on the concept
93 that if the waveforms at a station for two events are very similar (e.g. have high coherency) up to
94 a given dominant frequency, then the distance separating these events is small relative to the
95 seismic wavelength at that frequency (e.g., Geller and Mueller, 1980; Poupinet et al., 1984).

96 For detailed seismicity analysis, precise, differential times between like-phases (e.g., P and S) for
97 similar events can be measured using waveform correlation methods. Differential times from a
98 sufficient number of stations for pairs of similar events allows high-precision, relative location
99 between the events, usually maintaining the initial centroid of the event positions (Waldhauser and
100 Ellsworth, 2000; Matoza et al., 2013; Trugman and Shearer, 2017).

101 NLL-coherence uses waveform similarity directly to improve relative location accuracy without
102 the need for differential time measurements or many stations with waveform data. The method
103 assumes that high coherency between waveforms for two events implies the events are nearly co-
104 located, and also that all of the information in the event locations, when corrected for true origin-
105 time shifts, should be nearly identical in the absence of noise. Then, stacking over probabilistic
106 locations for nearby events can be used to reduce the noise in this information and improve the
107 location precision for individual, target events. We measured coherency as the maximum,
108 normalized cross-correlation between waveforms from one or more stations for pairs of events
109 within a specified distance after NLL-SSST relocation (2 km in this study). We take the maximum
110 station coherence between the target event and each other event as a proxy for true inter-event
111 distances and thus as stacking weights to combine NLL-SSST location probability density
112 functions (PDF's) over the events. In effect, this stack directly improves the hypocenter location
113 for each target event by combining and completing arrival-time data over nearby events and
114 reducing aleatoric error in this data such as noise, outliers and missing arrivals.

115 See Lomax and Savvaidis (2022) and Lomax and Henry (2023) for more discussion and details,
116 while NLL-SSST-coherence processing parameters used in this study are available on Zenodo at
117 the link <https://doi.org/10.5281/zenodo.10260849> (Lomax, 2023).

118

119

120

121 **Text S3: Focal mechanism determination**

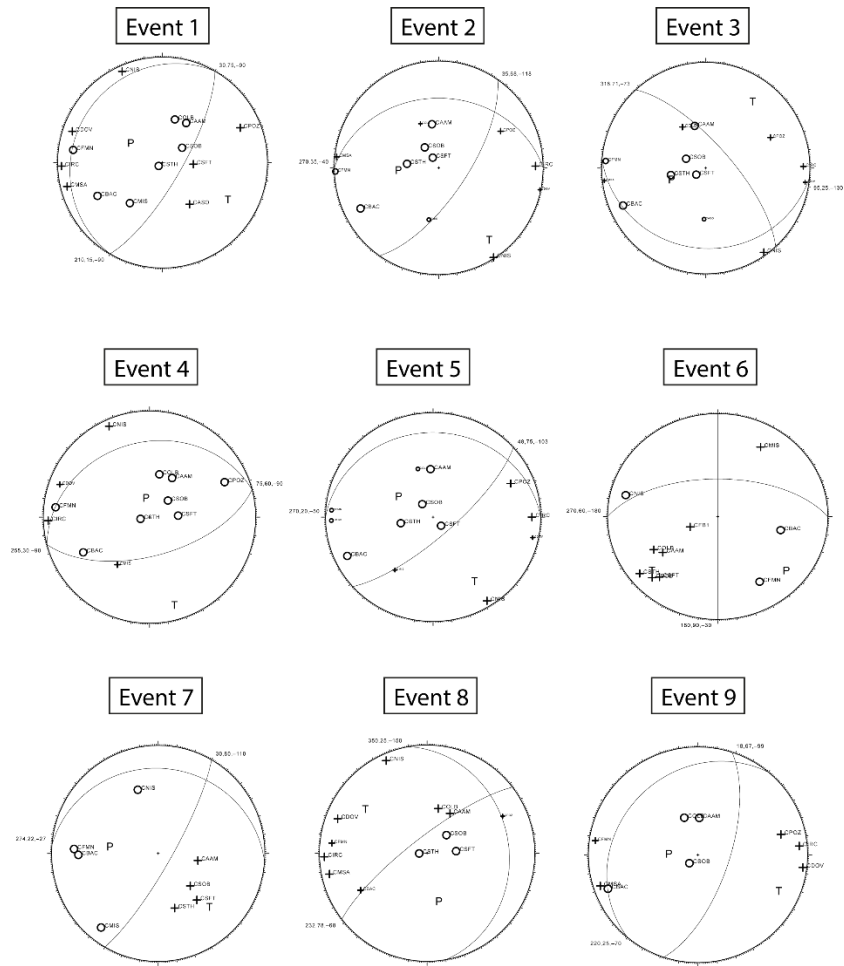
122 To determine in detail the fault geometry highlighted by the larger magnitude events from the mid
123 of August until the beginning of October 2023, we computed the focal mechanisms with the code
124 FPFIT (Reasenber, 1985) for 7 onshore events with duration magnitude larger than 3.6, and the
125 two larger magnitude events occurring offshore (See Figure 4). We estimated the polarity of the
126 first P-arrival as measured on velocity sensors of the INGV network by considering only stations
127 at a maximum epicentral distance of 8 km. An average of 11 P-polarities are available for each of
128 the analyzed events. We used the locations, for computing azimuth and take-off angles as the ones
129 obtained by the SSST-waveform coherence method assuming the same 1D velocity model used
130 for earthquake locations. The best fault-plane strike, dip and rake angles for each event can be
131 found in Table S1 together with the plot of the polarities on the focal sphere in Figure S3.

132

Event	Date	Time	Lat (°)	Long (°)	Depth (km)	Md	Strike F1/F2 (°)	Dip F1/F2 (°)	Rake F1/F2 (°)	Nb polarity
1	18/08/2023	04:09:59.42	40.8292	14.1487	2.4	3.2	30 / 210 ± 10	75 / 15 ± 3	-90 / -90 ± 5	14
2	18/08/2023	04:18:05.68	40.8300	14.1395	2.4	3.6	35 / 270 ± 0	68 / 35 ± 15	-118 / -40 ± 20	13
3	18/08/2023	04:22:49.91	40.8280	14.1388	2.1	3.1	95 / 318 ± 3	25 / 71 ± 8	-130 / -73 ± 15	13
4	07/09/2023	17:45:28.84	40.8295	14.1480	2.5	3.8	75 / 255 ± 3	60 / 30 ± 5	-90 / -90 ± 5	12
5	22/09/2023	09:02:00.02	40.8285	14.1415	1.8	3.0	48 / 270 ± 5	75 / 20 ± 13	-103 / -50 ± 15	13
6	26/09/2023	07:10:29.59	40.8063	14.1117	3.4	3.3	270 / 180 ± 3	60 / 90 ± 15	-180 / -30 ± 10	10
7	27/09/2023	01:35:34.39	40.8173	14.1553	2.9	4.2	30 / 274 ± 23	80 / 22 ± 8	-110 / -27 ± 25	8
8	02/10/2023	20:08:26.74	40.8297	14.1482	2.5	4.0	232 / 350 ± 10	78 / 25 ± 8	-68 / -150 ± 5	12
9	16/10/2023	10:36:21.14	40.8253	14.1420	1.8	3.6	18 / 220 ± 13	67 / 25 ± 5	-99 / -70 ± 40	9

133

134 **Table S1:** Location information of the larger magnitude events and description of the two planes in terms
135 of strike, dip and rake from focal mechanisms together with the uncertainties. Events are numbered
136 according to figure 4. Number of used polarities are reported for each event.



137

138

139 **Figure S3:** Focal mechanism solutions of the larger magnitude events with the polarity measurements
 140 projected on the focal sphere. Events are numbered according to figure 4.

141

142 **Caption for Movie S1.**

143 The video provides a 3D view of the 2014-2023 seismicity at the Campi Flegrei caldera, rotating
144 the view along a E-W oriented horizontal axis.

145

146 **Caption for Movie S2.**

147 The video provides a 3D view of the 2014-2023 seismicity at the Campi Flegrei caldera, rotating
148 the view along the azimuth.

149

150 **Caption for Movie S3.**

151 The video provides a 2D view of the yearly seismicity at the Campi Flegrei caldera, using the
152 same representation of Figure 2.

153

154